NASA Contractor Report 165821

Stereo Electro-Optical Tracker Study for the Measurement of Model Deformations at the National Transonic Facility

Richard J. Hertel and Kent A. Hoilman

ITT Aerospace/Optical Division
Fort Wayne, IN 46801

CONTRACT NAS1-16580

JANUARY 1982

NASA
National Aeronautics and Space Administration

Langley Research Center
Hampton, Virginia 23665

1. Report No.	2. Government Accession No.	3. Recipient's Catalog No.
NASA CR-165821		

4. Title and Subtitle	5. Report Date
Stereo Electro-Optical Tracker Study For the Measurement of Model Deformations at the National Transonic Facility	January 1982
	6. Performing Organization Code

7. Author(s)	8. Performing Organization Report No.
Richard J. Hertel and Kent A. Hoilman	
	10. Work Unit No.

9. Performing Organization Name and Address	11. Contract or Grant No.
ITT Aerospace/Optical Division 3700 E. Pontiac St. P.O. Box 3700 Fort Wayne, IN 46801	NAS1-16580
	13. Type of Report and Period Covered
12. Sponsoring Agency Name and Address National Aeronautics and Space Administration Washington, DC 20546	Contractor Report
	14. Sponsoring Agency Code

15. Supplementary Notes

Langley Technical Monitor: David Gray
Final Report

16. Abstract

This study examines the effects of model vibration, camera and window non-linearities, and aerodynamic disturbances in the optical path on the measurement of target position. The study examines window distortion, temperature and pressure changes, laminar and turbulent boundary layers, shock waves, target intensity and, target vibration. A general computer program was developed to trace optical rays through these disturbances.

The use of a Charge Injection Device (CID) camera as an alternative to the image dissector camera was examined.

17. Key Words (Suggested by Author(s))	18. Distribution Statement
Model Deformation Stereographic Measurement Electro-Optical Tracker National Transonic Facility	Unclassified - Unlimited Distribution

19. Security Classif. (of this report)	20. Security Classif. (of this page)	21. No. of Pages	22. Price
Unclassified	Unclassified		

For sale by the National Technical Information Service, Springfield, Virginia 22161

LIST OF TABLES

TABLE OF CONTENTS

LIST OF FIGURES

STEREO ELECTRO-OPTICAL TRACKER STUDY FOR THE MEASUREMENT OF MODEL DEFORMATIONS AT THE NATIONAL TRANSONIC FACILITY

RICHARD J. HERTEL AND KENT A. HOILMAN

SUMMARY

Model deformations must be measured if aerodynamic parameters are to be accurately determined. A report[1] recently completed investigated the feasibility of using a stereo tracker system to measure deformations in the National Transonic Facility. The present study investigates the influence on the stereo tracker system by the unique conditions found in the NTF. None of the conditions examined, (i.e., shock waves, boundary layers, pressure, temperature, vibration, and optics) will prevent meaningful deformation measurement provided care is taken in system design and the data is post-processed.

The use of a CID type system was examined and found to be inadequate for deformation measurement. Even with the expected technology advances, the proposed image dissector camera will remain superior in the near future.

A computer program was developed to trace virtually any ray through the complex tunnel conditions. The program will handle shock waves, boundary layers, pressures, temperatures, nonhomogeneous index of refraction, and optics of any conic section or polynomial of sixth order or less. This program approaches the goal of a universal ray trace program capable of handling any tunnel condition or ray geometry.

---

[1] Hertel, Richard J.: Study of a Stereo Electro-Optical Tracker System for the Measurement of Model Aeroelastic Deformations at the National Transonic Facility. NASA CR-159146, 1979.

INTRODUCTION

The primary purpose of this study was to investigate the effects on measurement accuracy of vibration, camera and window non-linearities and potential disturbances in the system optical path. Therefore, a detailed understanding of the system is not required but a familiarity with the general data gathering process will be helpful. The Stereo Electro-Optical Tracking System (SETS) measures the position of light emitting targets on a wind tunnel model by tracking the targets with two or more image dissector cameras located in the floor of the wind tunnel. These cameras or trackers are capable, under computer control, of measuring the brightness of a selected position of the scene. By measuring scene brightness of several areas the location of the targets can be determined. The exact target location is found by an iterative process which converges on the center of the target image and does no- rely on a single measurement or on a well defined target image. The location or positions of targets as measured by two or more trackers are combined in a stereo algorithm to determine true target position. Each tracker is capable of locating 1700 targets per second. Table 1 lists some of the SETS characteristics. Figure 1 shows a typical tracker configuration and its mounting arrangment. The inside of the tracker enclosure will be maintained at room temperature and atmospheric pressure.

Figure 2, 3, and 4 show the location in the tunnel for the six possible trackers. All of the trackers will be mounted below the model. All targets on the model are viewed by at least two trackers. Small luminous targets will be built into the model and controlled by the SETS electronics. Each target will be activated only when the trackers are viewing it. The entire system will be under computer control thus allowing the targets to be measured many times in any order.

176 61208 78

Table 1

SETS Characteristics

Sensed Volume	0.8m by 1.4m by 0.5m
Target Sources, Number	5 to 50
, Type	Light-Emitting Diode
, Size	0.5mm diameter
Model Deformation at Target Location	± 20mm maximum
Sensor Position Deviation Detection	0.05mm all axes
Model Vibration Limits	± 12.5mm at 20 Hz ± 5mm at 50 Hz ± 1.25mm at 200 Hz
Target Sampling Interval (Single Target Location)	590 microseconds, typical
Target Sampling Rate	1695 targets per second, typical
Sensor Tube Type	ITT F4012, S20 photocathode
Sensor Environment Control	70°F Dry Air at 130 psi (NASA Supplied) Electrical Heating
Tracking Electronics	Digital, in Tracker head
Calibration, geometric	Area map, prior to test
Pre-Test Reference	Targets on Stable Portion of model
Data Processor Type	MODCOMP
Data Storage	Magnetic Tape
Control/Display	CRT Display/Keyboard
Hard Copy	Line Printer/Plotter

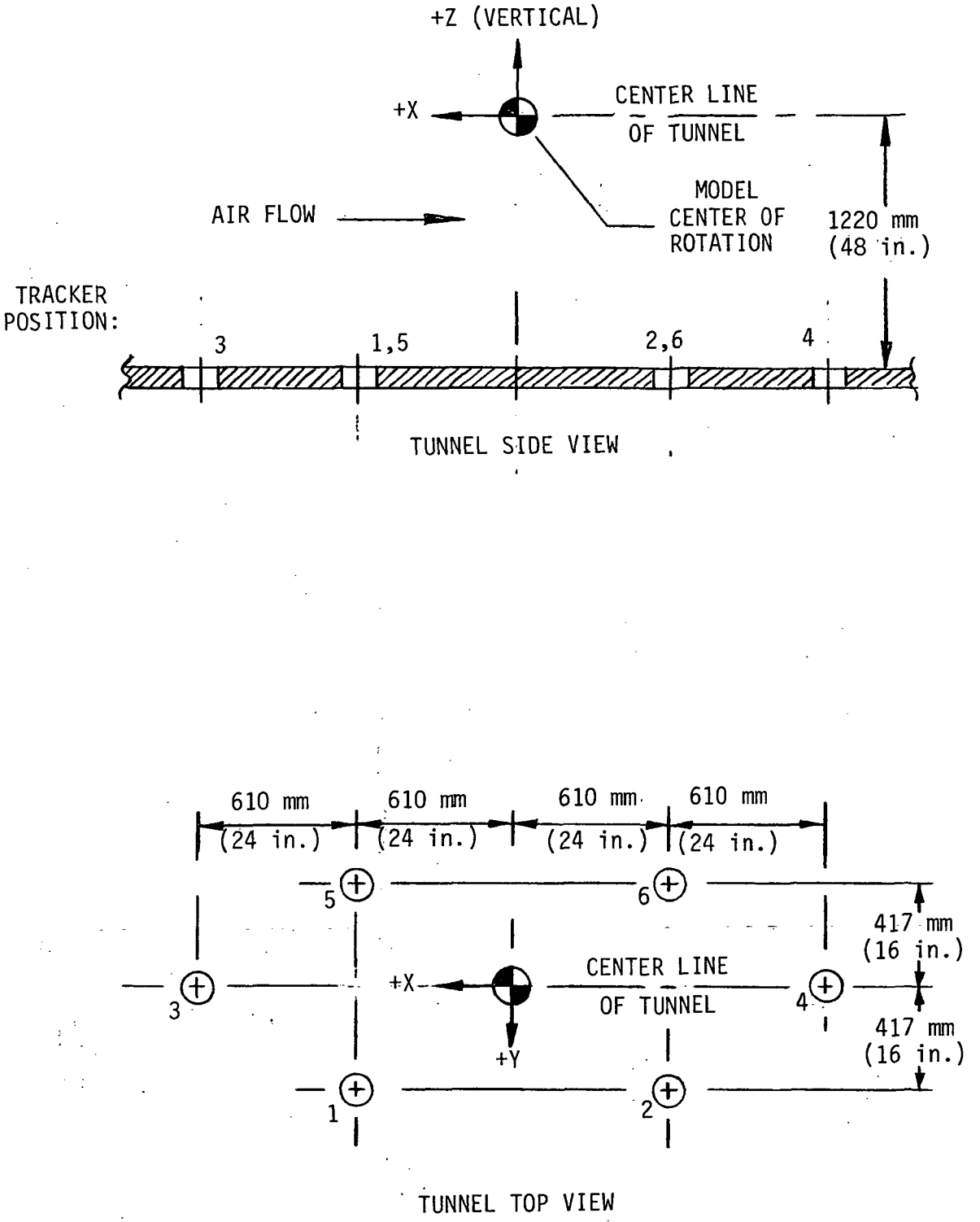

FIGURE 1 TUNNEL AXES AND TRACKER POSITION

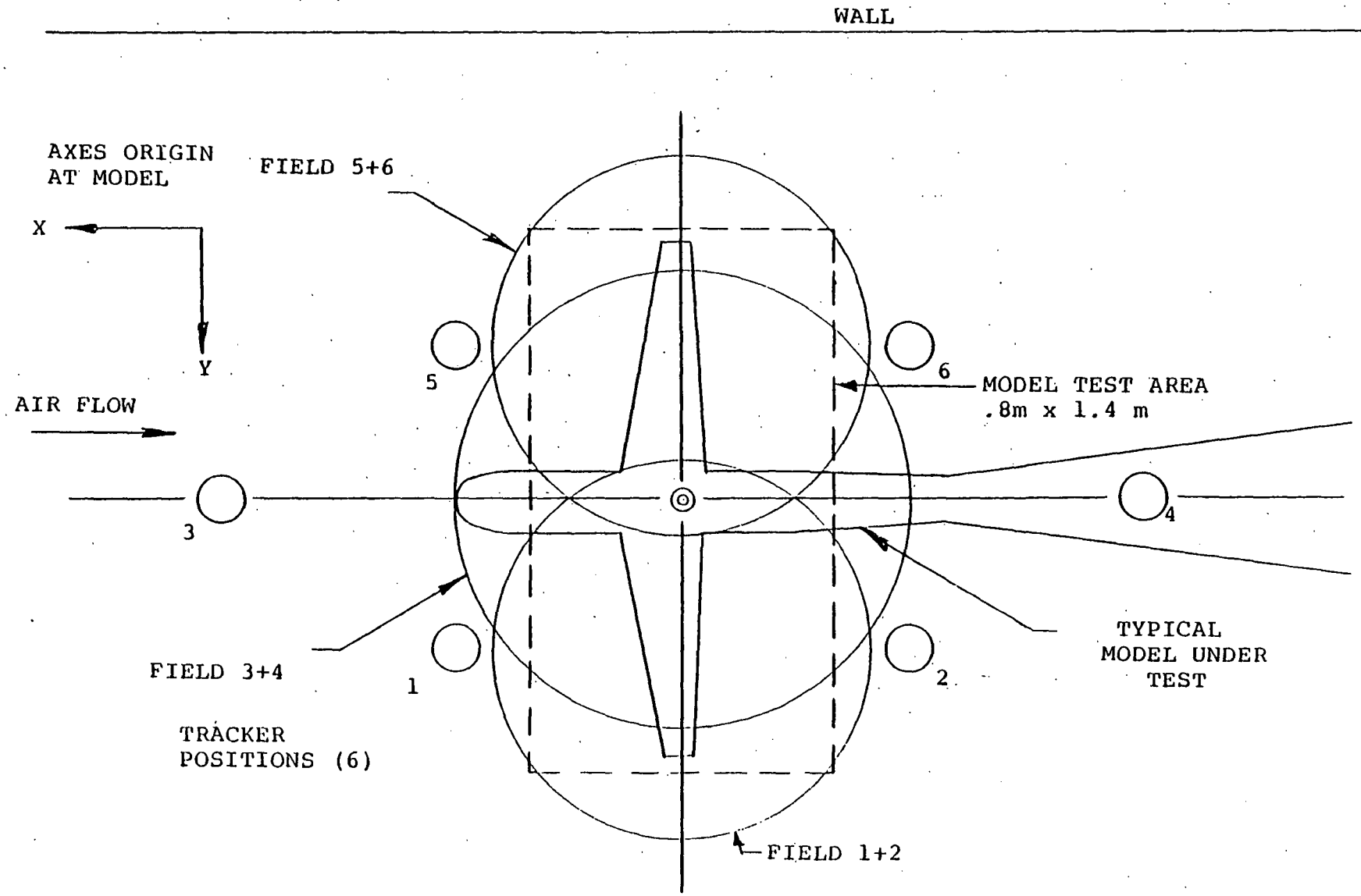

FIGURE 2 TRACKER AND FIELD LOCATIONS

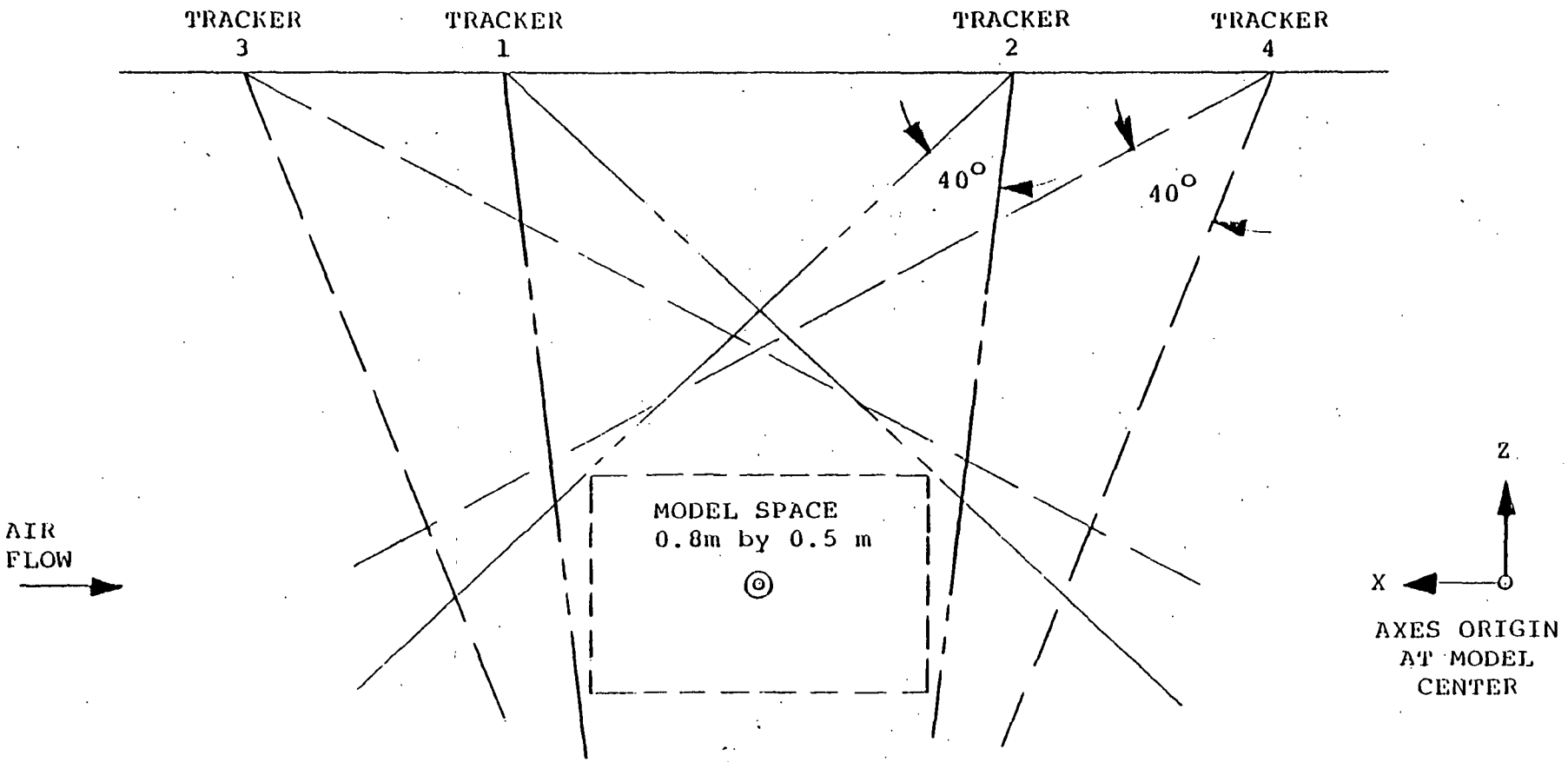

FIGURE 3 TRACKER COVERAGE OF MODEL SPACE IN XZ PLANE

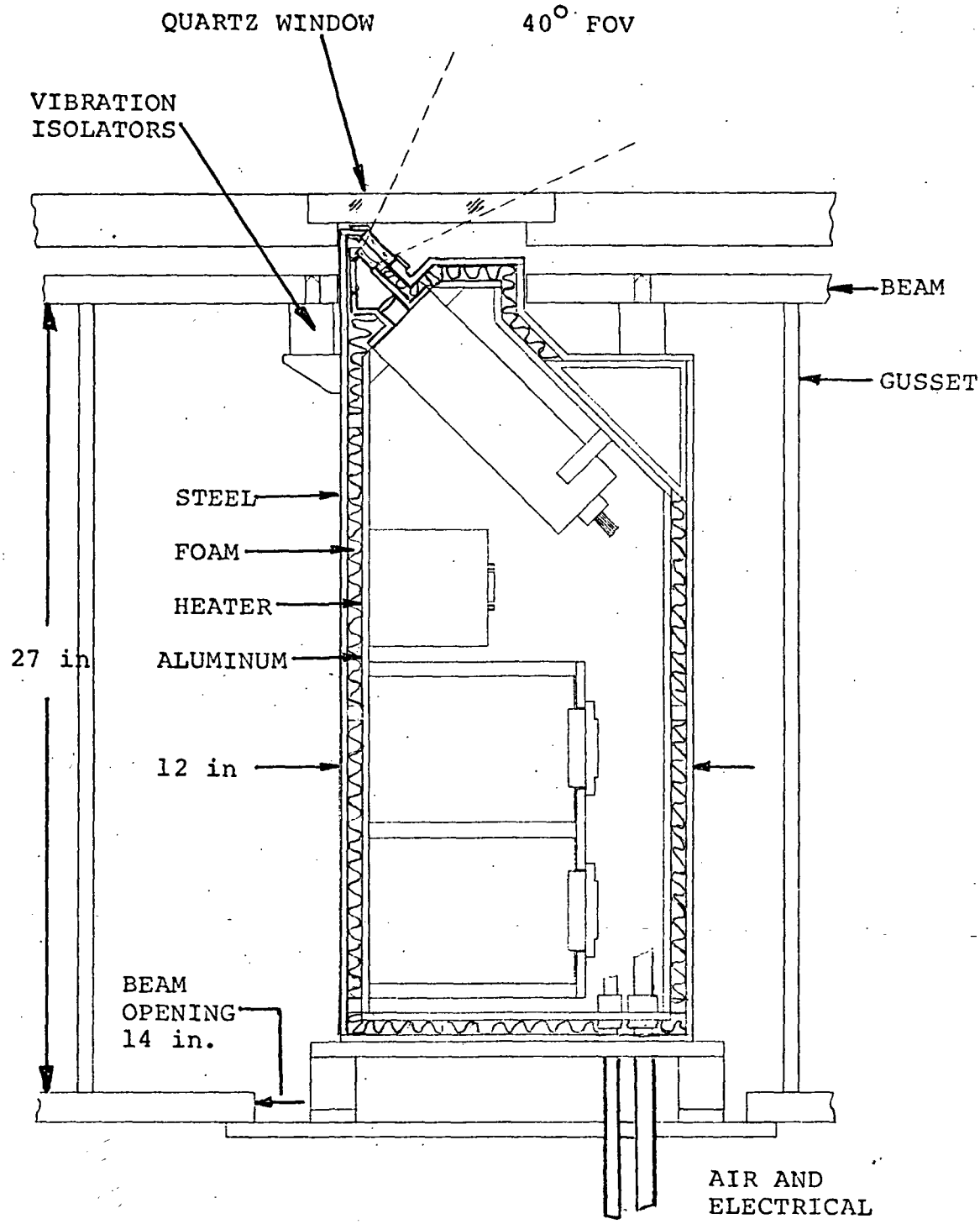

FIGURE 4. MULTI-TARGET TRACKER ASSEMBLY

ERROR SOURCES

Successful operation of the SETS requires that the trackers accurately measure the position of each model target in the wind tunnel environment which includes vibration of targets and trackers, extremely low temperatures, high static pressures, and potentially significant disturbances in the optical path of the cameras which result naturally from operation of the wind tunnel.

Eight separate areas of concern have been identified and are examined in this section. Some areas prove to be no problem. Some simply require the correct system design to minimize them. Some require that the data be corrected in a post processing step. All of the areas are manageable and should allow successful operation. This is summarized in Table 2.

Table 2. Error Summary

Area Investigated	Action Necessary		
Error Source	No Problem	System Design	Correction Required
Window Effects	X	X (tilt)	
Tunnel Pressure & Temperature			X
Laminar Boundary Layer Effects	X		
Turbid Boundary Layers	X	X (Target Size)	
Shock Wave Effects			X*
Vibration			X*
Targets		X	

*System Performance Limiting Effect.

Tunnel Window Effects

Window effects upon the optical measurement are due to the abrupt difference in index of refraction between the window and tunnel atmosphere. This difference coupled with the finite thickness of the window, the window curvature due to temperature and pressure, and the off-normal incidence of the camera line of sight cause a deviation in the optical path between the camera and the model.

Window Focus Effects

The curvature of the window by temperature or pressure introduces a small amount of additional optical power, $A\rho$, to the system.

$$A\rho = (n - 1)/r_1 + (1 - n)/r_2 - t(n - 1)\ (1 - n)/(n\ r_1\ r_2)$$

where n = index of refraction of the window, quartz 1.4581

t = thickness of the window

r_1 = inner radius of curvature

$r_2 = r_1 + 1$ = outer radius of curvature

When the window is concave on the model side, r_1 and r_2 are positive valued.

According to the data provided by NASA, the radius of curvature of a 1-inch thick window having a temperature gradient of +85°F across its faces is 37950.66414 inches. (Center sag is 110 microinches.)

$$\begin{aligned} A\rho &= (1.4581 - 1.)/37950.66414 \\ &\quad + (1. - 1.4581)/37951.66414 \\ &\quad - (1)(0.4581)(-0.4581)/(1.4581)(37950.)(37951.) \\ &= 4.18\ \text{E-10 inches}^{-1}\ \ (1.65\ \text{E-11 mm}^{-1}) \end{aligned}$$

$A\rho$ is the reciprocal of the focal length of the window "lens".

$$1/A\rho = 2.39\ \text{E+9 inches}\ (6.08\ \text{E+10mm})$$

This is a very weak lens. The camera optics are approximately 16mm focal length or $A\rho = 0.06mm^{-1}$. Temperature deformation of the window does not appear to be a significant factor affecting focus.

Pressure changes also cause the window to sag. The sag is 33 microinches, typical, to 54 microinches maximum according to NASA data. These sags are one-half or one-third those introduced by the temperature gradient. Again no significant focus effects are expected.

Window Displacement Effects

Figure 5 shows a ray incident on the window at an angle θ. This angle causes the ray path to be displaced from a straight line by an amount d.

$$d = t \sin\theta \left(\frac{1}{(1 - \sin^2\theta)^{\frac{1}{2}}} - \frac{n_1}{(n_2^2 - n_1^2 \sin^2\theta)^{\frac{1}{2}}} \right)$$

If the window tilts, θ changes by a small amount $d\theta$. The sensitivity of d to changes in θ is:

$$\frac{\partial d}{\partial \theta} d\theta = \frac{\partial}{\partial \theta} \left(t \sin\theta \left(\frac{1}{(1 - \sin^2\theta)^{\frac{1}{2}}} - \frac{n_1}{(n_2^2 - n_1^2 \sin^2\theta)^{\frac{1}{2}}} \right) \right) d\theta$$

$$= 19.2 \text{ mm/radian at } \theta = 35°$$
$$n_1 = 1.00298$$
$$t = 25 \text{ mm}$$

The objective of the measurement process is to locate the targets within 150 micrometers uncertainty. Therefore, the maximum tilt during any series of target measurements is:

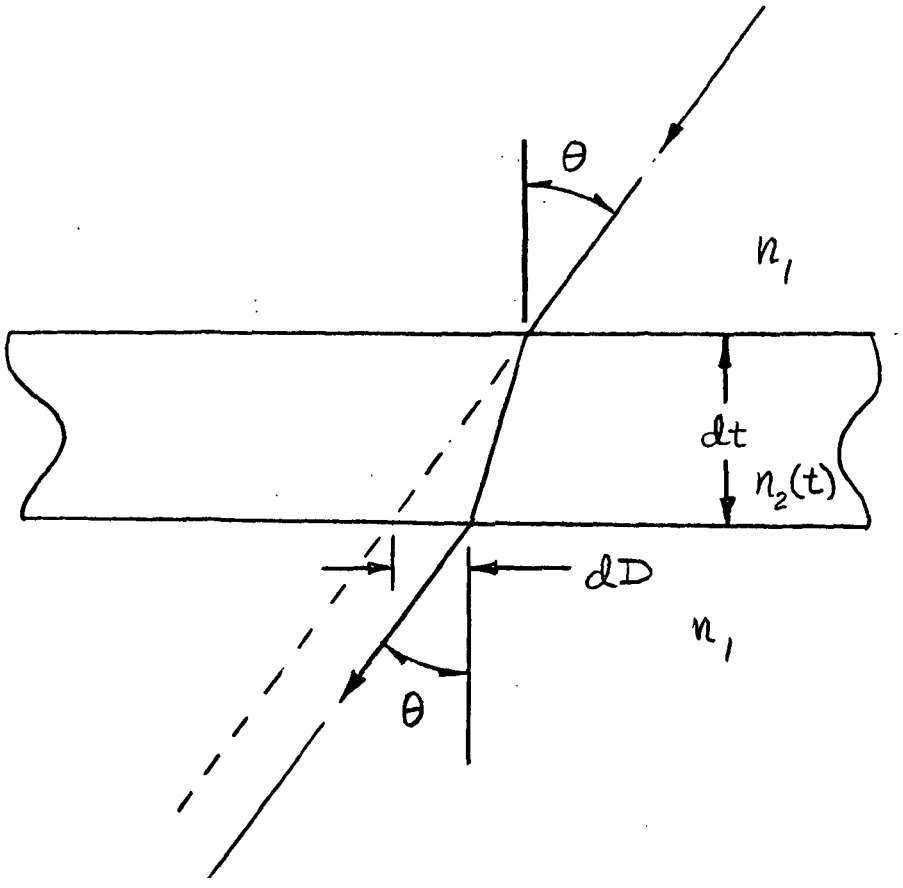

$$\frac{dD}{dt} = \text{SIN}\,\theta \left[\frac{1}{(1 - \text{SIN}^2\,\theta)^{\frac{1}{2}}} - \frac{n_1}{(n_2^2 - n_1^2\,\text{SIN}^2\,\theta)^{\frac{1}{2}}} \right]$$

FIGURE 5 Refraction at Test Section Window

$$\Delta\theta_{max} << \frac{150\ \mu m}{19.2 mm}\ \text{radian} = 7.8\ \text{mrad}$$

There is no reasonable estimate of the likely tilts available at this time.

The window must also have parallel faces. If the window has a wedge cross section, displacements of the window in the plane of the tunnel wall will cause changes in d.

$$\frac{\partial d}{\partial t}\, dt = 0.27\, dt \qquad \theta = 35°$$

$$n_1 = 1.00298$$

$$n_2 = 1.4581$$

The maximum thickness change must be less than:

$$\Delta tm << \frac{150\ \mu m}{0.27} = 550\ \mu m$$

over the maximum likely lateral displacement range. If 10 mm is used as the largest displacement range, then the maximum wedge angle is an easily-achieved value:

$$\alpha_m << \frac{.55}{10} = 3°$$

Tunnel Pressure and Temperature

During set up and initial target acquisition, the tunnel will be at normal atmospheric pressure and room temperature. During actual data runs, the tunnel may be cooled and pressurized. Both cooling and pressurizing the gas in the tunnel increases its density and thereby increases its optical index of refraction. This increase in the medium surrounding the model makes the model appear larger and distorted.

176 6/108 10

The index of refraction of nitrogen varies with the temperature and pressure by the following formula:

$$n - 1 = \frac{(n_o - 1)}{(1 + 0.00366\ t)} \frac{P}{760}$$

where n_o = 1.000298 for 0°C and 760 mm Hg.
thus $n(-195°C, 9\ atm) = 1.00937$
$n(+95°C, 1\ atm) = 1.00022$

If the tracker is maintained at a constant pressure and temperature while the tunnel is pressurized and cooled, the maximum image change possible is produced. The interaction at the tunnel window can be reduced for calculation purposes to a single interface where Snell's law ($n\sin\Theta = n'\sin\Theta'$) applies. Using the tunnel geometry and a FOV of 40° for the tracker, the effects can be calculated. Figure 6 shows the situation for a tracker located at position 4. The 40 degree FOV allows a model 1600 mm long to be viewed.

Table 3 gives the angles and dimensions as viewed from the tracker for the two extreme tunnel conditions. The model appears to grow by approximately 4 percent. This scale change is not linear. The scale change of 4 percent can be followed by the tracker as discussed in the next paragraph; however, the non-linearity introduced must be removed by the data analysis routines.

If the tunnel conditions change at such a rate that the target with the maximum optical induced motion is just tracked, then that rate is the upper limit on change allowable for the gas temperature and pressure. If the capture range of the tracker is a 200 x 200 μm square and the target is viewed 30 times per second, the maximum motion is then 5600 μm/s on the tube face or (using a 250 x scale factor) approximately 350 mm/s on the model. Thus, the temperature and pressure must change from room

FIGURE 6 TYPICAL OPTICAL GEOMETRY

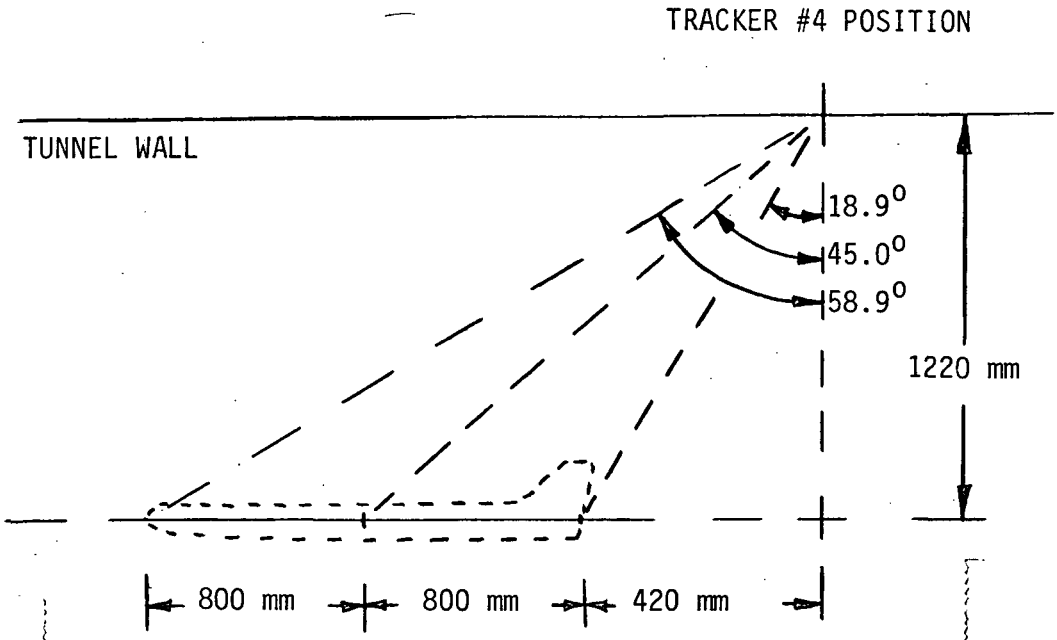

Table 3

ANGLE AND LENGTH CHANGES

Target Location (degrees)		Apparent Length (mm)		
Θ Before	Θ After	Θ Before	ℓ After	Δℓ Change
18.99 (tail)	19.181	420.0	424.4	4.4
30.00	30.310	704.4	713.2	8.8
40.00	40.452	1023.7	1040.2	16.5
45.00 (center)	45.539	1220.0	1243.2	23.2
50.00	50.644	1453.9	1487.6	33.7
58.87 (nose)	59.770	2020.0	2093.6	73.6

Before Conditions: +95C, 1 atm

After Conditions: -195C, 9 atm

See Figure 7 for angle and length definitions.

ambient to LN_2 and 9 atmospheres in less than 1/4 second to cause loss of track. This will not be an operational limitation, as cooling requires hours.

In order to calculate more accurately the influence of pressure and temperature changes, the simple optical model of Figure 6 was modified to that in Figure 7. The tracker is assumed to be on the tunnel centerline (position no. 4 of Figure 2) and tilted at an angle of 50° in the X-Z plane. The 50° angle provides coverage of the entire model with a reasonably well-centered image. The tracker optics are positioned 20 mm outside the tunnel window and consist of an ideal 16 mm lens.

The model of Figure 7 was programmed in Fortran IV. Program ITO traces rays from the image in the tracker to the object in the tunnel. Program OTI traces rays from the object in the tunnel to the image in the tracker. This ray cannot be traced directly and is found by an iteration technique. Tables 4 and 5 are sample printouts from the OTI program. Tables 6 and 7 are sample printouts from the ITO program. The scale is the size of the output variable divided by the size of the input variable. Thus for the ITO program, the scale is the size of the image divided by the size of the model for the specific image and object conditions used. The scale varies from 0.013 (the image is 1.3 percent of the size of the model at the tail to 0.004 at the nose). This scale is in the x axis of the tunnel only. For the OTI program, the scale is the object size divided by the image size. If a particular ray is traced in both directions, the object and image points should match and the scales will be reciprocals.

When the tunnel is pressurized to 9 atmospheres and cooled to LN_2 temperatures, the increased density of the gas makes the model appear approximately 4 percent larger. The size increase is not uniform or linear over the model. The tail grows

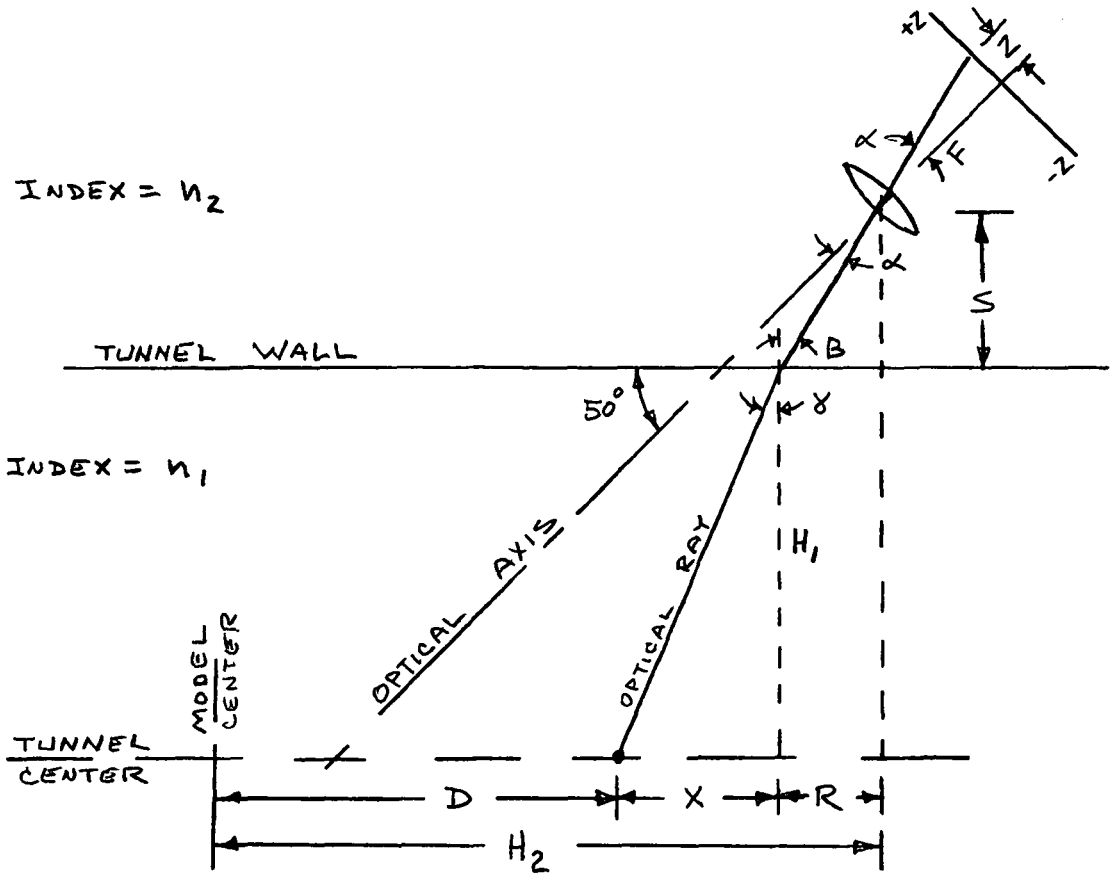

Camera Optical Axis = 50°

TAN α = Z/F

TAN γ = X/H_1

n_2 Sin β = n_1 Sin γ

$\alpha + \beta = 40^{\circ}$

Tan β = R/S

H_1 = 1200 mm

S = 20 mm

H_2 = 1200 mm

F = 16 mm

n_1 = 1.00937 (9 atm, LN_2 temp)

n_2 = 1.00022 (1 atm, Room temp)

Figure 7. Simple Optical Model

Table 4

OBJECT TO IMAGE RAY TRACE

Room Temperature, One Atmosphere

F= 16.00 N1= 1.00022
S= 20.00 N2= 1.00022
H1= 1220.00 H2= 1220.00

O	X	R	Z	SCALE
800.000	413.226	6.774	6.2343636	.013324738
700.000	511.613	8.387	4.9678335	.012027740
600.000	610.000	10.000	3.8220496	.010905266
500.000	708.387	11.613	2.7805390	.009935856
400.000	806.774	13.226	1.8296814	.009093046
300.000	905.161	14.839	.9581341	.008355141
200.000	1003.548	16.452	.1563694	.007689238
100.000	1101.936	18.065	-.5836632	.007114530
.000	1200.323	19.677	-1.2688375	.006593227
-100.000	1298.710	21.290	-1.9050233	.006132603
-200.000	1397.097	22.903	-2.4973021	.005721092
-300.000	1495.484	24.516	-3.0500727	.005345345
-400.000	1593.871	26.129	-3.5671563	.004997730
-500.000	1692.258	27.742	-4.0518961	.004692078
-600.000	1790.645	29.355	-4.5072336	.004417419
-700.000	1889.032	30.968	-4.9357758	.004158974
-800.000	1987.419	32.581	-5.3398180	.003922462

Table 5

OBJECT TO IMAGE RAY TRACE

LN_2 Temperature, 9 Atmospheres

F= 16.00 N1= 1.00937
S= 20.00 N2= 1.00022
H1= 1220.00 H2= 1220.00

O	X	R	Z	SCALE
800.000	413.158	6.842	6.1782265	.013424873
700.000	511.524	8.476	4.9016590	.012127876
600.000	609.887	10.113	3.7459483	.011003971
500.000	708.247	11.753	2.6943588	.010035038
400.000	806.602	13.398	1.7330987	.009196520
300.000	904.953	15.047	.8507072	.008457780
200.000	1003.298	16.702	.0375786	.007810626
100.000	1101.637	18.363	-.7143929	.007230043
.000	1199.969	20.030	-1.4120929	.006718159
-100.000	1298.295	21.705	-2.0614152	.006275177
-200.000	1396.612	23.388	-2.6674588	.005856037
-300.000	1494.920	25.080	-3.2345853	.005484104
-400.000	1593.220	26.780	-3.7666178	.005152925
-500.000	1691.509	28.491	-4.2669029	.004857063
-600.000	1789.787	30.213	-4.7383709	.004572868
-700.000	1888.054	31.946	-5.1835918	.004329681
-800.000	1986.309	33.691	-5.6048603	.004094124

Table 6

IMAGE TO OBJECT RAY TRACE

Room Temperature, One Atmosphere

F= 16.00 N1= 1.00022
S= 20.00 N2= 1.00022
H1= 1220.00 H2=1220.000

Z	R	X	O	SCALE
6.00000000	7.060	430.682	782.258	76.355
5.00000000	8.344	508.986	702.670	82.837
4.00000000	9.739	594.079	616.182	90.198
3.00000000	11.260	686.883	521.856	98.560
2.00000000	12.926	788.498	418.576	108.142
1.00000000	14.758	900.240	305.002	119.165
.00000000	16.782	1023.702	179.516	131.985
-1.00000000	19.030	1160.830	40.140	147.000
-2.00000000	21.541	1314.027	-115.568	164.743
-3.00000000	24.365	1486.291	-290.657	185.907
-4.00000000	27.564	1681.421	-488.985	211.462
-5.00000000	31.218	1904.293	-715.511	242.554
-6.00000000	35.431	2161.273	-976.704	281.091

Table 7

IMAGE TO OBJECT RAY TRACE

Room Temperature, One Atmosphere

F= 16.00 N1= 1.00022
S= 20.00 N2= 1.00022
H1= 1220.00 H2=1220.000

Z	R	X	O	SCALE
6.17822647	6.842	417.378	795.780	75.305
4.90165901	8.476	517.039	694.485	83.533
3.74594831	10.113	616.885	593.002	92.212
2.69435883	11.753	716.950	491.297	101.343
1.73809875	13.398	817.271	389.331	110.980
.85070705	15.047	917.884	287.068	120.947
.03757860	16.702	1018.828	184.470	131.464
-.71439290	18.363	1120.141	81.496	142.484
-1.41209292	20.030	1221.858	-21.889	153.923
-2.06141520	21.705	1324.021	-125.727	165.860
-2.66745377	23.388	1426.674	-230.062	178.439
-3.23458529	25.080	1529.854	-334.933	191.418
-3.76661777	26.780	1633.600	-440.381	204.993
-4.26690292	28.491	1737.960	-546.451	219.067
-4.73837090	30.213	1842.978	-653.191	233.679
-5.18359184	31.946	1948.698	-760.643	249.011
-5.60486031	33.691	2055.168	-868.859	264.819

about 1 percent while the nose grows over 9 percent. This change becomes important when the model's absolute position is calculated. The apparent shifts caused by the density change could possibly be interpreted as model motion caused by air loadings or structural changes. The local scale factor between object and image also increases with gas density. The scale increases vary from 1 percent at the tail to 9 percent at the nose. The scale is important when vibrations are being considered or when measurement precision is determined. The absolute position of the target is not necessary if a vibration measurement is made. Only changes in its position relative to some reference is needed. If the model grows, the reference position simply shifts. If the scale changes, the vibration measurement changes proportionately.

The distortions introduced by pressure and temperature must be removed in the analysis of the data. The correction can be calculated provided the tunnel conditions are known.

The optical model of Figure 7 can be described by the following equation:

$$D = H_2 \frac{H_1 Q}{\sqrt{1 - Q^2}} - \frac{S \tan C - \frac{SZ}{F}}{1 + \frac{Z}{F} \tan C}$$

where $$Q \equiv \frac{n_1 F \sin C}{n_2 \sqrt{Z^2 + F^2}} - \frac{n_1 Z \cos C}{n_2 \sqrt{Z^2 + F^2}}$$

C = angle of camera
Z = image location
D = target location
F = focal length
H_1 = tunnel height
H_2 = tunnel length
n_1 = index in tunnel
n_2 = index outside tunnel

The scale number is then the derivative of this equation and is:

$$\frac{dD}{dZ} = \frac{-H_1}{\sqrt{1 - Q}} \frac{d\Theta}{dZ} - \frac{Q^2 H_1}{(1 - Q^2)\sqrt{1 - Q^2}} \frac{d\Theta}{dZ} - \frac{S/F}{1 + \frac{Z}{F} \tan C}$$

$$- \frac{\frac{S^2}{F} - S \tan C) \tan C}{(1 + \frac{Z}{F} \tan C)^2 F}$$

where: $$\frac{d\Theta}{dZ} = \frac{- \cos C}{n_1 \sqrt{Z^2 + F^2}} - \frac{Z (F \sin C - Z \cos C)}{n_2 (Z^2 + F^2) \sqrt{Z^2 + F^2}}$$

Laminar Boundary Layers

Boundary layers will be present on the wind tunnel test section walls and on the surface of the model. These layers have the effect of changing the angle of rays passing through them and of displacing the rays. This can be demonstrated by approximating a boundary layer as a series of uniform layers.

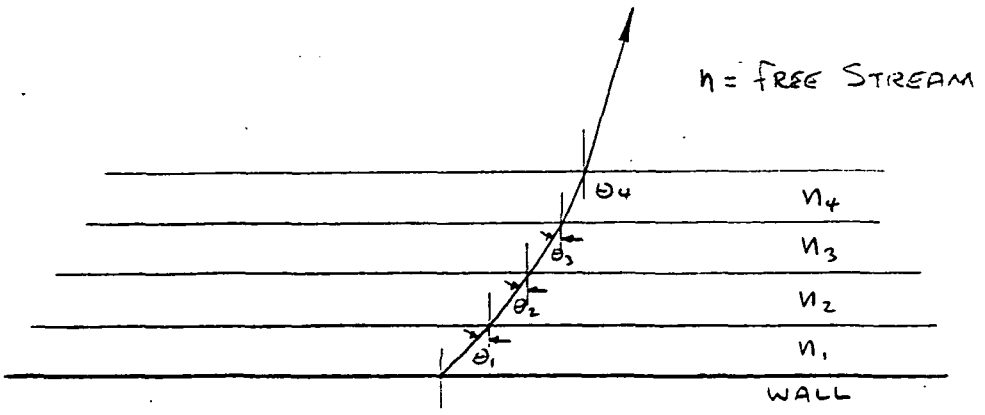

Figure 8. Layer Model for Boundary Layers

For each interface between layers Snell's law applies:

$$n_1 \sin \theta_1 = n_2 \sin \theta_2$$

Thus for a series of layers:

$$n_1 \sin \theta_1 = n_2 \sin \theta_2 = n_3 \sin \theta_3 = n_4 \sin \theta_4 = \text{etc.}$$

For a series of parallel layers, the product of the index of refraction and the sine of the angle is constant. Thus, the conditions of the first and last layer are all that are needed to compute the angle. Figure 8 shows the typical ray path through a boundary layer.

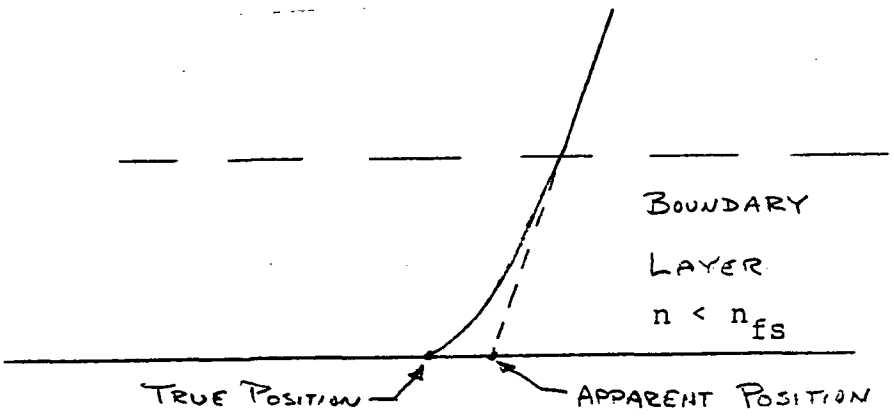

Figure 9. Light Path through Boundary Layer

The ray emerges from the boundary layer at a different angle and the light source appears to be shifted from its actual location. These two effects, angle and shift, must be handled separately.

When viewing a light source immersed in a boundary layer, the source appears shifted as shown in Figure 9. For a single tracker, the shift is along the surface, but for a pair of trackers and a stereo transform, the shift is also into the surface. Either component of the shift depends on the ray angle, the boundary layer thickness, and the index gradient in the boundary layer. The index can be computed using the Gladstone - Dale constant K:[2,3]

$$n - 1 = K\rho \quad \text{where } \rho \text{ is density}$$

The density for boundary layers can be related to temperature by:[3,4]

$$\frac{\rho_1}{\rho_2} = \frac{T_2}{T_1}$$

The temperature can be found by:[4]

$$\frac{T_2}{T_1} = \left[1 + \frac{\gamma - 1}{2} \varepsilon M^2\right]^{-1}$$

---

[2] Stine, H: Application of Scattering Theory to the Measurement of Turbulent Density Fluctuations by an Optical Method. NACA Technical Note 3719.

[3] Liepmann, H.W.: Deflection and Diffusion of a Light Ray Passing Through a Boundary Layer. Douglas Aircraft Report No. SM-14397, 1952.

[4] Dommash, D.: Airplane Aerodynamics. Pitman Publishing Corp., 1967.

where ε is the boundary layer recovery factor. Thus, for a worst-case condition there is a 25 percent change in the quantity n - 1.

$$\frac{\rho_1}{\rho_2} = \frac{T_2}{T_1} = \left(1 + \frac{\gamma - 1}{2} \varepsilon M^2 \right)^{-1} = 0.7472$$

where $M = 1.2$ (Tunnel maximum)[5]

$\varepsilon = 1.0$ (Total Recovery)

$\gamma = 1.47$ (Nitrogen at -181°C)

The thickness of the boundary layer can be calculated by:[4,6,7]

$$t = \frac{5.2\ X}{\sqrt{R_N}}$$

where $R_N = 120 \times 10^6$ (tunnel maximum)

$X = 1$ meter, (typical model fuselage length) so that:

$$t = \frac{5200}{10954} = 0.47 \text{ mm}$$

A worst-case situation can now be calculated by assuming the maximum index variation takes place at the free stream edge of the boundary layer and the entire boundary layer is at the lower index value.

The shift in apparent target position can now be calculated as shown in figure 10. The shift along the surface is:

---

[4] Dommasch, D., Airplane Aerodynamics. Pitman Publishing Corp., 1967.

[5] Nickes, O.W.: Status and Operational Characteristics of the National Transonic Facility. AIAA 10th Aerodynamic Testing Conference paper, 1978.

[6] Hansen, A.G.: Fluid Mechanics. John Wiley and Sons, Inc., 1967.

[7] Shames, I.H.: Mechanics of Fluids. McGraw-Hill, 1962.

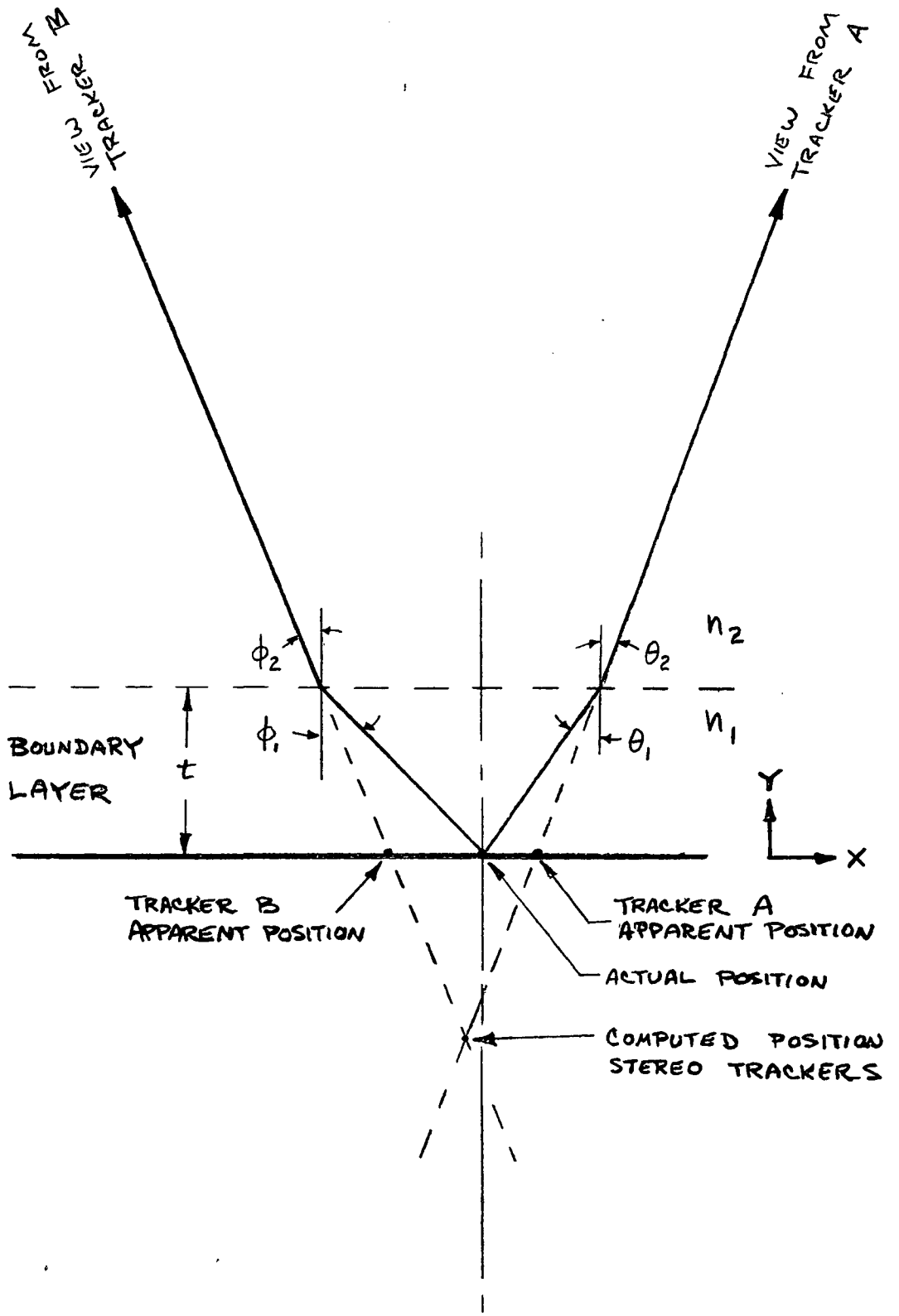

FIGURE 10 Target Shifts due to Boundary Layer

$$S_A = t(\tan \theta_1 - \tan \theta_2) \qquad \text{(Camera A)}$$
$$S_B = t(\tan \phi_1 - \tan \phi_2) \qquad \text{(Camera B)}$$

The shift seen by a stereo pair is:

$$S_H = \frac{\ell}{X + 1} - \frac{\ell}{Y + 1} \qquad \text{(horizontal along surface)}$$

$$S_V = \frac{\ell \cos \phi_2 \cos \theta_2}{\sin(\phi_2 + \theta_2)} \qquad \text{(vertical into surface)}$$

where $\ell = t(\tan \theta_1 + \tan \phi_1)$

$X = \tan \theta_2 / \tan \phi_2$

$Y = \tan \theta_1 / \tan \phi_1$

$n_1 \sin \theta_1 = n_2 \sin \theta_2$

$n_1 \sin \phi_1 = n_2 \sin \phi_2$

$20° < \theta_2 < 60$

$20° < \phi_2 < 60$

$n_1 = 1.00700$ (maximum index in boundary layer)

$n_2 = 1.00937$ (maximum index in tunnel)

This produces a worst-case shift of 7 μm along the model when viewed by one tracker. When viewed by two cameras, the worst-case condition is a shift into the surface of 4.5 μm and 1.0 μm along the surface. These values are for extreme conditions and a simple optical model. For typical wing targets, the shift will be less than 1 μm when viewed by one tracker and less than 2 μm when viewed by a stereo pair due to the reduced angle of view and smaller boundary layer thickness.

The multiple layer model of Figure 8 was programmed. In order to ensure accuracy, all ray tracing variables are double

percision variables. The product of the index and the sine of the angle is computed from the length calculations and never converted back to an angle. This prohibits buildup of errors due to use of the trigometric functions. Several versions of the program were developed for various approximations of the index gradient.

Figure 11 shows the index of refraction in the boundary layer for several different approximations. The zero order approximation assumes the index in the entire boundary layer is the minimum index value. Thus, a ray bends sharply at the boundary edge and is straight from then on. The first order approximation assumes a first order polynomial, or linear variation for the index. A ray curve goes through the boundary layer and intersects the aircraft surface with only 40 percent of the shift indicated by the zero order trace. The second order ray trace assumes a second order polynomial, or parabola, for the index variation. This is the equation used by Shames[7] to represent the velocity in the layer. This model leads to about a 10 percent boundary layer thickness error. Using this formula, the ray trace yields a shift of only 25 percent of the zero order ray trace.

The actual index variation depends on the density, not the velocity. Using Bernoulli's equation for compressible flow, the density can be approximated. The Bernoulli equation is:

$$\frac{\gamma}{\gamma - 1} \frac{p}{\rho} + \frac{V^2}{2} = \text{constant}$$

In boundary layer, the pressure is practically independent of distance from the surface and can be assumed a constant (p = constant). Thus:

$$\rho = \frac{C_1}{(C_2 - V^2)}$$

---

[7] I. H. Shames, Mechanics of Fluids, McGraw-Hill, 1962.

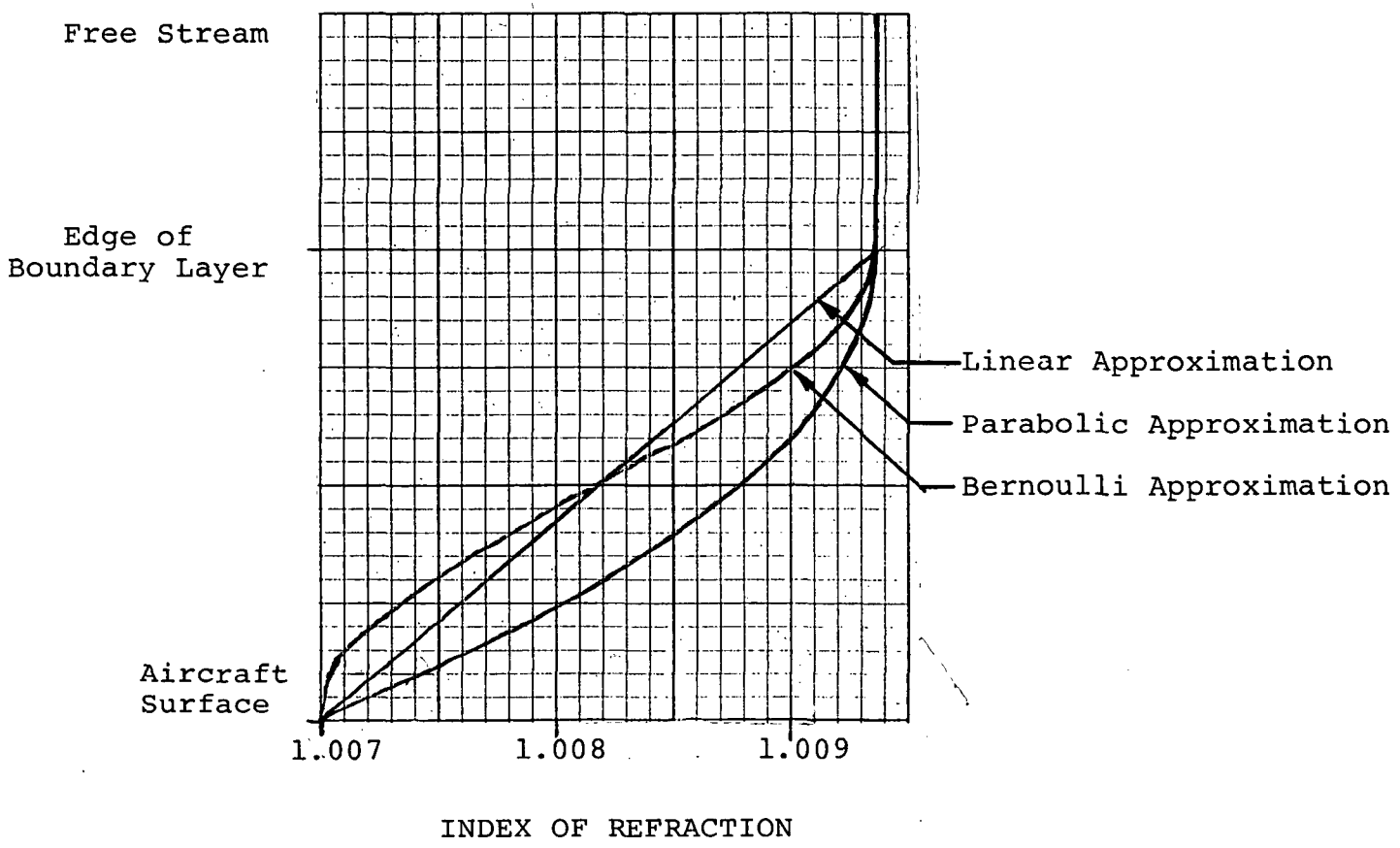

Figure 11. Index of Refraction Models

176 61108 17

where C_1 and C_2 are constants. The boundary conditions normalized to free stream conditions are:

for	V = 1.0 (free stream)	ρ	= 1
	V = 0 (surface)	ρ	= 0.747
	V = 1.0	$\frac{d\rho}{dv}$	= 0

Thus: $C_1 = 2.955$

$C_2 = 3.955$

The final relationship between position (Y) and index of refraction (n) can be found by combining the Bernoulli approximation, the parabolic velocity approximation, and the Gladstone - Dale equation.

$$n = K\rho + 1$$

where

$$\rho = \frac{2.955}{3.955 - V^2}$$

where

$$V = 2Y - y^2$$

Figure 12 shows the path of a ray through the boundary layer for each model of index. The worst-case shift for a change from +95°C at 1 atmosphere to -195°C at 9 atmospheres can be computed. The constant index model of figure 10 yields a 7 μm shift. The linear index model yields a 4.2 μm shift. The parabolic index model yields a 3.0 μm shift. The Bernoulli index model yields a 4.3 μm shift. These shifts are along the surface when viewed by a single tracker. When viewed by a stereo pair of trackers as shown in Figure 10, the shift along the surface is approximately one fifth as large but there is a shift into the surface of approximately one-half the single tracker value. These shifts are small when compared to the 150 μm allowable error for the system. Thus, laminar boundary layers will not degrade the system.

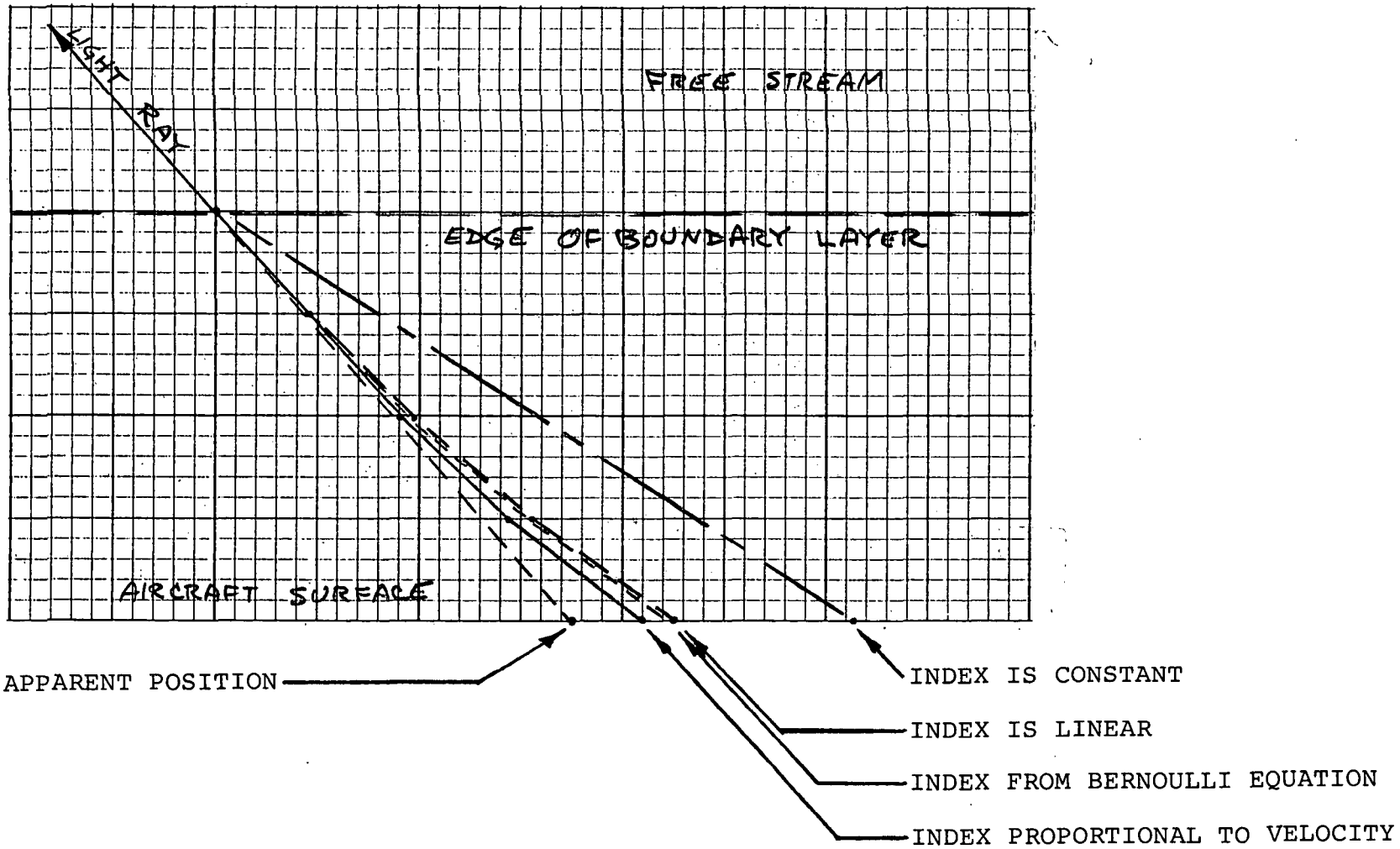

FIGURE 12. Ray Path through Boundary Layer

Boundary layers on the tunnel window will cause an insignificant shift in the focus. The analysis of the tunnel window's effect on focus can be applied to each layer of figure 8. The thickness and the index change in each layer is small resulting in an insignificant focus shift.

Turbulent Boundary Layers

Turbulent boundary layers may develop on the model and the tunnel window. The influence of turbulent boundary layers can be calculated by the following equation:[8]

$$\Theta = K B \rho \sqrt{t}$$

where

Θ is the resolution limit
K is 2.47 rad $ft^{5/2}$/slug
ρ is free stream air density
t is boundary layer thickness
B is scattering parameter

The boundary layer thickness can be calculated by:

$$t = \frac{0.37x}{R_N^{1/5}}$$

where $x = 1 \times 10^3$ mm (typical fuselage length)
$R_N = 120 \times 10^6$ (tunnel maximum)

The value of B can be found from wind tunnel measurements:[8]

$$\frac{B}{\rho t} = 0.04 \text{ for } M = 1.2$$

---

[8] Wolfe, W.: Handbook of Military Infrared Technology. 1965.

Thus, the thickness (t) is 8.9 mm or 0.03 feet. The value of Θ is then 1.23×10^{-3} radians. This indicates that for collimated light, 85 percent of the total energy will be imaged into a spot 1.23×10^{-3} radians in diameter. In this situation, the light is not collimated and the boundary layer can be at the target or at the tunnel window.

If the boundary layer on the tunnel window is turbulent, then the expected resolution on the model 1000 mm distant is approximately 1 mm. This is twice the target size and considerably larger than the 150 μm permissible position error. Fortunately, the system does not require that the target is resolved to 150 μm accuracy, but requires that the centroid of its image is located to that accuracy. The tracking process of sampling the scene brightness in a converging measurement sequence locates the target accurately even though the boundary layer precludes sharp spatial resolution. The loss in resolution will slow the convergence when near the final location by changing the slope of the error detection curve. The larger image will also tend to linearize the detection curve thus speeding up the first few cycles of the convergence. The absolute image size expected is quite acceptable.

If the boundary layer is on the model, it produces a random target shift of approximately 10 μm. This is well below the 150 μm allowable error and should cause no problems. There may be a slight fluctuation in the intensity due to the angular change in the viewing of the target, but this is expected to be insignificant due to the extremely small angular change (0.07 degree) and the 100 μs time scale of the tracker intensity measurement process.

176 64 0822

Shock Wave

Shock waves can be modeled as a single refracting surface with the index of refraction changing at the shock wave. The relationship between the density of the mdeium prior to and after a shock is:[8,9]

$$\frac{\rho_2}{\rho_1} = \frac{(\gamma + 1)\, M^2 \sin^2 \Theta}{2 + (\gamma - 1)\, M^2 \sin^2 \Theta}$$

where:

ρ_1 = density after the shock
ρ_2 = density before the shock
M = Mach number
Θ = angle of shock to air flow
γ = 1.47 for nitrogen at -195°C, 9 atm

The maximum density ratio is 1.33 for a normal shock (Θ = 90°) and M = 1.2, which is the tunnel maximum. This yields n_2 = 1.00937 ahead of the shock and n_1 = 1.01246 behind the shock. For a ray incidence of 45°, the deviation will be 0.175 degrees causing a target of 1000 mm distance to shift 3.05 mm. Fortunately, this worst-case condition will not exist for any reasonable aircraft model.

A much more realistic situation is for a shock at 45° to the flow. This yields density ratios of 1.015 and n_1 of 1.00923 behind the shock. For a ray incident at 45°, the deviation will be 0.008 degree causing a target at 1000 mm to shift 138 μm. Any reduction in the angle of either the shock wave itself or the incidence of the light ray will reduce this value. The value of 1000 (range) is dependent on the actual location of the target. For typical wing mounted targets, a range of 700 mm is more reasonable, yielding a shift of only 97 μm.

If the shock is conical, then it acts as a lens and

---

[9] Domasch, D.: Airplane Aerodynamics. Pitman Publishing Corp., 1967.

causes a focus shift. The effective focal length of the shock can be calculated by:[10]

$$\frac{f}{x} = \frac{n_2 \tan \theta}{n_1 - n_2}$$

where:

f = focal length
x = distance from apex of shock
n_1 = index after shock
n_2 = index before shock
θ = shock angle

For a 45° shock at M = 1.2 and x = 700 mm, the focal length is 5×10^6 mm. The resulting shift can be calculated by:

$$\text{Shift} = x - \frac{xf}{x - f}$$

Thus, for typical wing targets (x = 700 mm) the shift is 97 μm in focus. This is well within the tracker's ability and can be ignored.

Vibrating Objects

The objective of the SETS is to measure deformation of wind tunnel models. This is done by measuring the position of targets placed on the model. Each target is measured by two or more trackers and the stereo transformation provides the correct X, Y, and Z position.

The SETS can measure target positions at a rate of 1700 targets per second. If 50 targets were placed on the model then each target would be measured 34 times every second (34 x 50 = 1700). With more targets, there would be less measurements

---

[10] Jenkins, F.: Fundamentals of Optics. McGraw-Hill Book Company, 1957.

every second and, conversely, there would be more measurements every second with less targets. If the model is stable, a simple average of the measurements would yield a target's position and hence the model deformation. The more measurements that are averaged, the less system noise and the less erroneous data points will affect the final position.

The big unknown in the system is stability. Care has been taken in the design of the NTF tunnel to provide stable conditions and tunnel operation will undoubtedly be optimized to provide the best conditions when data is taken. However, due to the extreme resolution of the SETS (150 μm of motion is maximum allowable), even this will not provide a non-moving model. Vibrations from the tunnel machinery and the model interacting with the air will cause the targets to move. The average position of the target must be measured such that the average model deformation can be found.

The exact vibration of the target can only be estimated at this time. The expected vibration spectrum is shown in Figure 13 and will be a combination of sine and random components. Low frequency motions will be due to the sting and supporting structure, while high frequency motions will be from the less massive model itself. The highest frequencies would be expected at the wing tips due to vibration. Random vibration will be generated from the turbulent boundary layers. Thus, any measurement scheme must handle sine and random components.

The SETS measures the target position by an interactive process that converges on the center of the target. Vibration during the time that a single measurement is being made slows the convergence but has little effect on the measured position due to the speed of the system.[11] Thus a single measurement

---

[11] Hertel, Richard J.: Study of a Stereo Electro-Optical Tracker System for the Measurement of Model Aeroelastic Deformations at the National Transonic Facility. NASA CR-159146, 1979.

is the instantaneous position of the target. The SETS acts like a strobe in that it freezes the target position at the moment of sampling. By examining these frozen position measurements, the average target position is obtained.

The stroboscopic concept is ideal in examining the SETS data. In the typical stroboscopic application, the object is vibrating at a much higher frequency than the sampling light source. This causes the objects motion to appear greatly slowed and in fact stopped if the two frequencies are multiples. The object's true motion is not measured but can be derived from the measurements if taken correctly. If the object has a single vibration frequency, sampling at two different rates is enough to deduce the motion. If many vibration frequencies are present then many more sampling rates are required. As long as the vibration is periodic and unchanging, and enough data is gathered, the original wave form can be reconstructed. The technique allows for slow sampling (compared to the signal) but requires long time periods (compared to the signal period) of observation. This stoboscopic technique is similar to that used in sampling oscilloscopes.

Most stroboscopic investigations and all sampling oscilloscopes are designed to reconstruct the waveform. This is more information than required for the SETS where only the average value of the waveform is needed. Thus, many of the restrictions mentioned earlier on sampling at many frequencies may not apply. An investigation of the sampling frequencies and the resulting errors was performed by assuming all vibration frequencies were possible and sampling using various techniques would be available.

The simplest mathematical model is to assume sine wave vibration and uniform sampling. A 50-Hz sampling rate was chosen as representative of a typical SETS data run (i.e., 34 targets

measured at 1700 samples/s). Two sampling techniques were investigated. The first method obtained its first sample at the zero point in the sine wave vibration and subsequent samples at 1/50th of a second intervals. The second method obtained its first sample at the positive peak in the sine wave vibration, and subsequent samples were at 1/50th of a second intervals. In both cases, the signal was sampled for one second and the 50 samples were averaged. The results are shown in Figure 14. The maximum errors occur when the vibration frequency is a multiple of the sampling rate and, thus, the two are synchronized. The minimum error occurs when the vibration frequency is not related to the sampling rate and errors less than 3 percent of the peak vibration motion are obtained.

A more complex sampling method would use multiple sampling rates, and the results are shown in Figure 15. Sampling was done at the rate of 20 per second and also at the rate of 30 per second. The curve shows similar peak errors to the single rate sampling technique. Peak errors occur when the vibration frequency is a multiple of either sampling rate and minimum errors occur when the vibration frequency is not related to either sampling rate. Multiple rates produce multiple frequencies where peak errors occur but have very little effect on the average value of the error curve. If the vibration frequencies present are distributed over the frequency range, there appears to be little advantage to either the single or the multiple sampling rate methods. If, however, the vibrational frequencies are concentrated at particular frequencies then a sampling scheme may be designed to minimize the errors.

If Gaussian noise is added to the sine wave vibration of the previous models, the sampling method becomes less of a factor in the error determination. Random noise introduces an error that is not removed by any sampling method and tends to mask the

Figure 14 Sampling at 50 Times per Second

Figure 15 Sampling at 20 and 30 Times per Second

errors present due to the sampling and vibration frequency resonances. In the SETS, random vibration can be expected to be a large component of the target motion. Thus, the error in the measured position will be largely dependent on obtaining as many samples as possible, and the sampling method will be of secondary importance.

If the time between samples is allowed to vary slightly, the overall error will be unaffected but the minimum and maximum error values will be brought closer together. If, instead of sampling at exactly 1/50th of a second intervals, the sampling is at intervals varying randomly between 1/40th and 1/60th of a second, the error curve peaks and valleys will be reduced. This is a direct consequence of the vibration frequency not being an exact multiple of the sampling rate. The SETS will automatically introduce some randomness into the sample interval due to the convergence technique used to collect data. Additional randomness could be introduced into the data collection if desired.

The discussion thus far has concerned vibration frequencies above the sampling frequency. For vibration below the sampling frequency, a different set of problems are present. For these low frequency vibrations several samples per cycle are possible, and the portion of the signal sampled can be reconstructed. Figure 16 shows a hypothetical situation where low frequency vibration is present. The measured position could be interpreted as consisting of a 0.225Hz and a 2-Hz vibration plus higher frequencies. The wave can be reconstructed, but due to the limited time of observation (1 second data run), only part of a cycle is present. If the data is averaged, the low frequency vibration (below 1 Hz) could lead to errors. These errors can be reduced if the data is analyzed for these low frequencies and corrections made. Hopefully, these low frequency vibrations will be small. If they are not small, and accurate corrections for

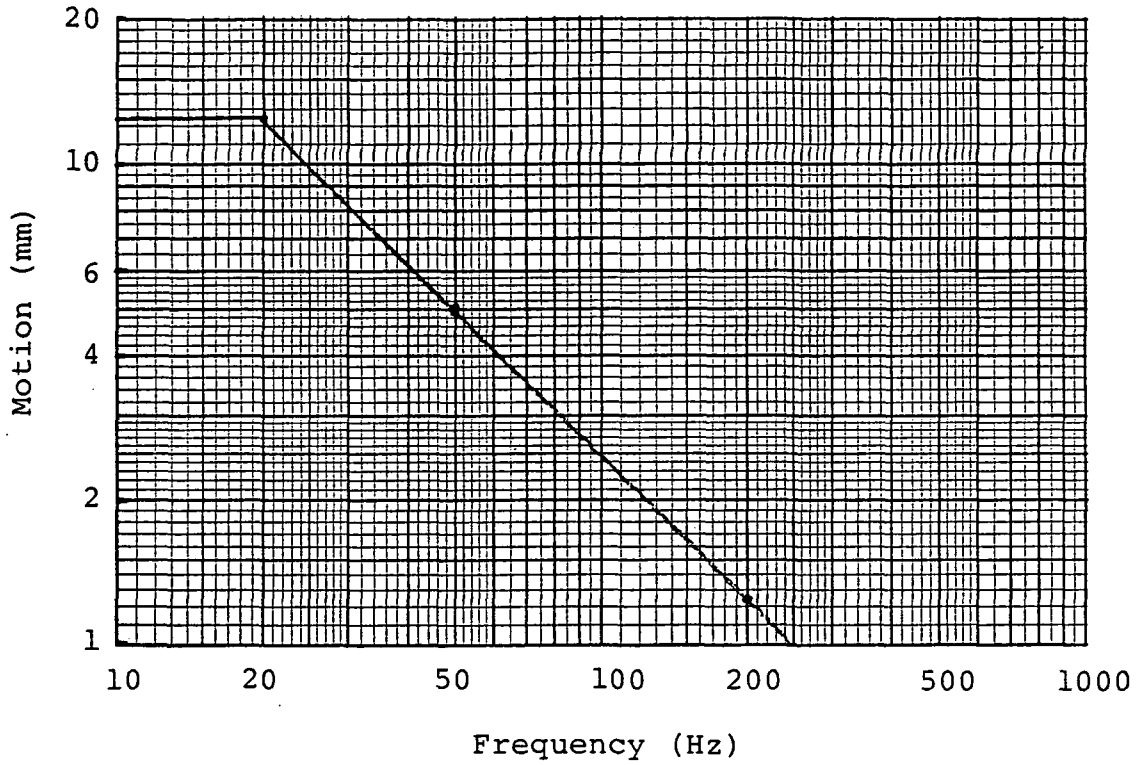

Figure 13 Vibration Envelope

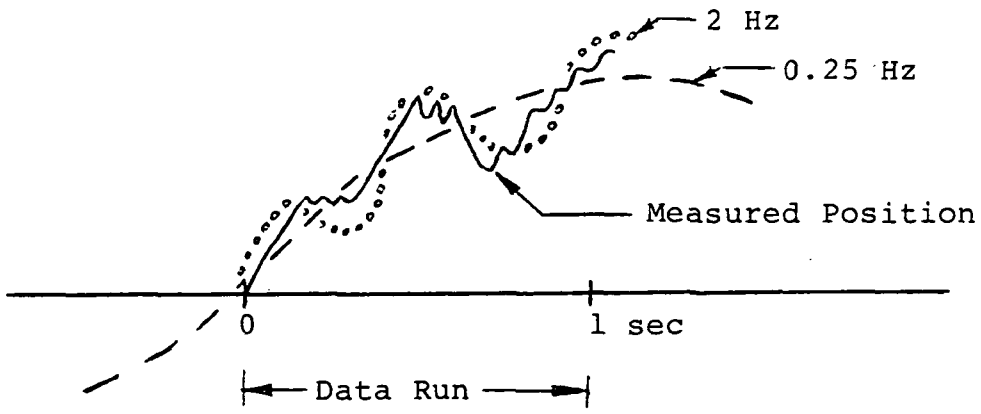

Figure 16 Low Frequency Motion

them are needed, the period of data collection must be lengthened to use data either before or after the one second data run.[12]

Target Characteristics[13]

Targets cannot be considered without also considering some aspects of target illumination and tracking method. The model can move in pitch, roll, and yaw over a substantial fraction of the tracker system field of view. Thus, the target appearance can change substantially. The ideal solution is a combination of targets, illumination, and tracking method which yields a position measurement accuracy independent of changes in

1. Target size - magnification
2. Target orientation - rotation
3. Target shape - distortion
4. Target illumination - magnitude, uniformity
5. Target contrast - stray light
6. Target focus - depth of focus
7. Target viewing angle - off normal view

---

[12]Each wind tunnel test will consist of a series of tunnel conditions and model attitudes. The tunnel will be allowed to stabilize after each change prior to data collection. Thus, the operation is a series of step and dwell operations. A typical SETS data run will be one second of data collection during the stable dwell period.

[13]Hertel, J. R.: Study of a Stereo Electro-Optical Tracker System for the Measurement of Model Aeroelastic Deformations at the National Transonic Facility. NASA CR-159146, 1979.

The target and its illumination must also be optically efficient in terms of power input to the illuminator for the signal needed at the camera.

Target Size

There are two general classes of targets; point and finite. Point targets are not resolved as a disc image by the camera and optics. Finite targets have a definable size, shape and even structure.

Point targets can be defined quantitatively as having an image whose size is less than one-third the size of the camera optical spread function. The section on camera optics estimated the radius of the spread function to be 10-20 μm plus a 0 to 8 μm term for depth of focus effects. Using the dimensions of Figure 2 and a 16 mm FL lens, the smallest demagnification is about 75 at a range of 1200 mm. The size of the target at the model is, therefore, 2 x 750 μm/3 = 500 μm or less diameter.

Target position for point targets is measured by making four samples in the vicinity of the target image. The position of the four samples is adjusted until all have equal signal amplitude.

Numerous types of finite targets can be considered. In general, finite targets require more image samples than point targets because of the range of sizes and possible orientations.

Two simple examples of finite targets are the white circle in a black surround or the black and white wedge as shown in Figure 17.

Since the model can move in range and pitch angle, these targets in the extreme can look like those shown in figure 18. A scanning method which is independent of these size and shape changes is a raster whose dimensions are greater than the maximum possible target size. The scanned data is then used to compute the center of brightness, assuming a uniform target. This method is time consuming if done by computer or complicated electronically if done by a dedicated hardware processor.

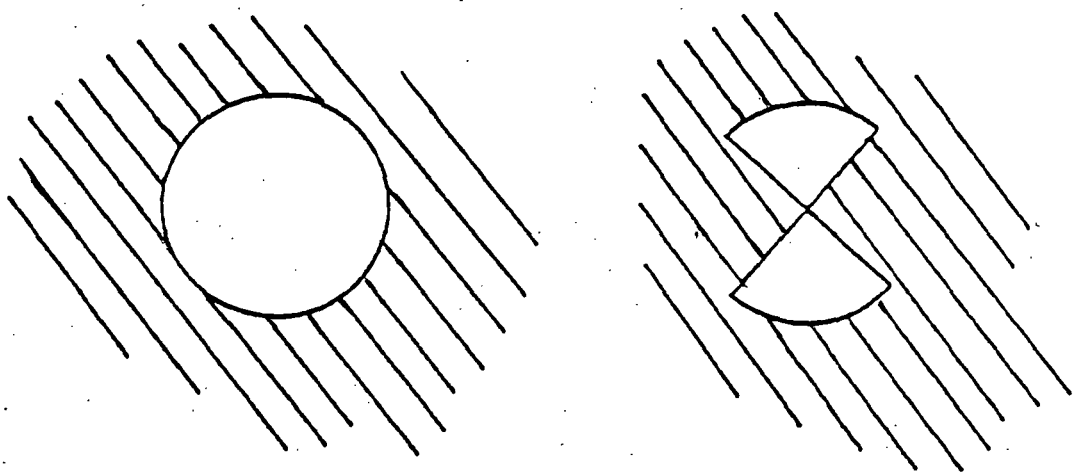

Figure 17. Two Examples of Finite Targets

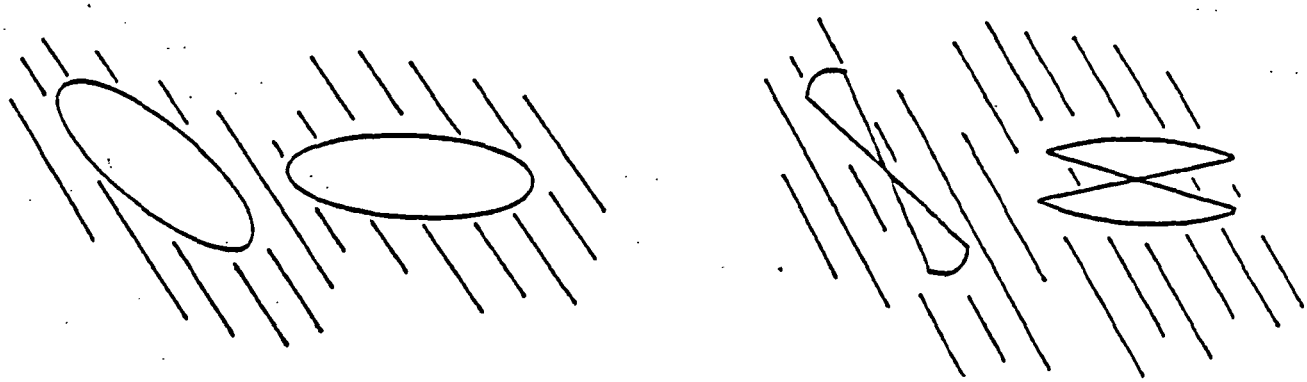

Figure 18. Finite Targets at Large Angles

A less complex or time consuming method uses a circular scan pattern. The method seeks the black-white edge crossings and adjusts the center of the scan circle until two pairs of edge crossings are each 180° apart. This method is sensitive to target rotation. The rotation must be known or measured before proper adjustment of the scan center occurs.

In general, finite targets require a tracking and measurement method insensitive to size and shape changes. Finite targets are best used where some useful information is conveyed by their size, shape, or pattern.

Active versus Passive Targets

Targets can be either active sources of light or passive reflectors of light. Active point targets such as light emitting diodes are optically very energy efficient. All the energy contributes to the source intensity. Fiber optic light pipes are a bit less efficient due to losses along the fibers and at the input coupling. Nonetheless, optical fibers viewed end on are potentially good targets.

Passive point targets, such as diffuse painted patterns, are optically very inefficient in this installation. Only a small fraction of the incident energy is reflected to the cameras. Passive point targets can be illuminated by a spot light that moves in step with the tracker as the tracker moves from target to target. Such a scheme would require either premapping of all nominal target positions versus angle of attack, or, real time computation of illuminator pointing angles. It is still necessary to illuminate an area larger than the passive target, since an allowance for pointing errors must be made.

The flux onto a target at normal incidence is given by

176 61208 32

$$F = B_o A \frac{4\pi f^2 SNR^2 M^2 Ke \varepsilon_1 \varepsilon_2}{S \Delta t}$$

where
$A = 1 \times 10^{-6}$ m^2, the area of a point target
$f = 2.8$, the focal ratio of the lens
$SNR = 30$, the signal-to-noise ratio needed in a typical system
$M = 125$, the demagnification between target and image
$K = 2.3$, the noise factor of the camera
$e = 1.602 \times 10^{-19}$ coulombs/electron
$\varepsilon_1 \varepsilon_2 = 1$, reflection and lens transmission factors
$S = 200$ μA/lumen, the camera sensitivity
$\Delta t = 20$ μs, the time to make one brightness sample

$$F = B_o A = \frac{4\pi(2.8)^2(30)^2(125)^2(2.3)(1.6 \times 10^{-19})\ (1)(1)}{(200 \times 10^{-6})\ (20 \times 10^{-6})}$$

$$F = 0.13 \text{ lumen}$$

The target is only 1×10^{-6} m^2 in area, yet the flux is 0.13 lumens. The illuminance must therefore be 1.3×10^5 lumen/m^2. This is the same as direct sunlight. For flood illumination of the 1 m^2 field of view at the model this is at least 8 kW of quartz-iodide lamps in housings with very efficient reflectors. For a moving spot of illumination using a 10 cm^2 area this is about 250 watt of quartz-iodide illumination with an f/2 projector lens.

A corner cube reflector used as a passive point target can be energy efficient. A collimated beam of light to a corner cube is reflected back along the same path to the source. A corner cube target does not exhibit the depth of focus effects previously mentioned because the source appears to be located at infinity. The two major problems with corner cubes are size and view angle. Also, it is not clear if millimeter sized cubes do not work at large angles (45°) of incidence.

In general, active point targets such as LEDS are perferred.

Target Contrast

Contrast between target and surrounding model is an important property. A point target tracker can, in principle, operate on low contrast targets. In practice, the background signal should be eliminated to minimize the dynamic range of the electronics and to remove the effects of background flux changes.

Let F_o, F_1, and F_2 be the average values for the background, sample 1, and sample 2 signals. Associated with each sample is a noise n_o, n_1, and n_2, each proportional to the square root of their respective signals. The track scan position error signal, E, is :

$$\varepsilon = C_1 \frac{(F_1 + F_o) - (F_2 + F_o)}{(F_1 + F_o) + (F_2 + F_o)} = C_1 \frac{F_1 - F_2}{F_1 + F_2 + 2F_o}$$

It is possible to remove the $2F_o$ term by making a measurement of the background signal. This additional measurement will add 20 to 60 μs to the single cycle time.

Removal of the $2F_o$ term does not completely solve the background problem. At null position, $F_1 = F_2$, the finite noise associated with each of the samples becomes important. The noise, e, about the null position is equal to:

$$e = C_1 \frac{(2n_o^2 + n_1^2 + n_2^2)^{\frac{1}{2}}}{F_1 + F_2 + (2n_o^2 + n_1^2 + n_2^2)^{\frac{1}{2}}}$$

If $F_o \approx F_1$, 50 percent contrast, then the position noise about null is at least $\sqrt{2}$ times greater than with zero background. As F_o becomes larger than F_1, a still lower contrast, then n_o, the noise in the background signal becomes the dominant[14] term.

---

[14] Image dissectors will respond to the 120 Hz ac flicker from incandescent or fluorescent lights. This can increase the b_o noise term considerably beyond the shot noise value.

1'16 C/208-34

If $F_o \leq 0.1\ F_1$, a condition corresponding to > 90 percent contrast, background measurement and subtraction is not necessary. If $F_o = 0.1\ F_1$, the noise about null is only 5 percent greater than the zero background case; an acceptable condition.

Tracker control loop gain depends upon the $2F_o$ term in the error signal equation. For $0 \leq F_o \leq 0.1\ F_1$, the change in loop gain is less than 1 dB, an acceptable value.

The limits on absolute background brightness and the needed target intensity can be estimated for a system using LED targets. The required signal-to-noise ratio for the difference between target and background is 30:1 RMS. This signal-to-noise ratio allows the center of the target to be located at $\pm$ 0.5 μm at the model for zero angle at attack and center of the field of view.

Let I_o and I_1 be the photocurrents entering the aperture of the image dissector due to the background and the target plus background. It is required that the signal-to-noise ratio of $I_1 - I_o$ be greater than or equal to 30. Since the image dissector is a shot noise limited device, the noise in each of the two photo currents is

$$i_o = \frac{ekI_o^{\frac{1}{2}}}{\Delta t} \quad \text{amperes}$$

$$i_1 = \frac{ekI_1^{\frac{1}{2}}}{\Delta t} \quad \text{amperes}$$

where

$e = 1.602 \times 10^{-19}$ coulombs/electron

$k = 2.5$, image dissector noise factor

Δt = sample time, 20 μs in this system.

$$SNR \doteq \frac{I_1 - I_o}{(i_o^2 + i_1^2)^{\frac{1}{2}}} = \frac{I_1 - I_o}{\frac{ek}{\Delta t}^{\frac{1}{2}} (I_1 + I_o)^{\frac{1}{2}}}$$

These equations assume no ac modulation of the background. If there is ac modulation, i_o becomes the rms value of the modulation. As calculated here, the equation gives the greatest dc I_o value that is tolerable. The noises are assumed to be uncorrelated and to add in quadrature.

Figure 19 is a plot of $I_1 - I_o$, the required target photo current versus background photo current I_o for SNR = 30 and t = 20 μs. An additional abscissa scale on the plot shows the maximum background luminance at the model for 2854 K tungsten illumination, f/2.8 lens and a 200 x 200 μm aperture in the image dissector. General office illumination is on the order of 100 lumen m^{-2} $steradian^{-1}$.

The extra scale on the ordinate axis gives the target source intensity to cause the signal photo current. This intensity is based upon a f/2.8 lens and a red LED. Red LED's produce 1×10^{-4} watts/steradian at 60 mA current, 25°C, and normal incidence.

Undoubtedly, there will be other sources of light used within the tunnel. These sources could be incandescent, fluorescent, or laser. They may even be turned on and off for various reasons and will probably operate from the ac line. It is prudent to make the tracking system as insensitive as possible to these sources.

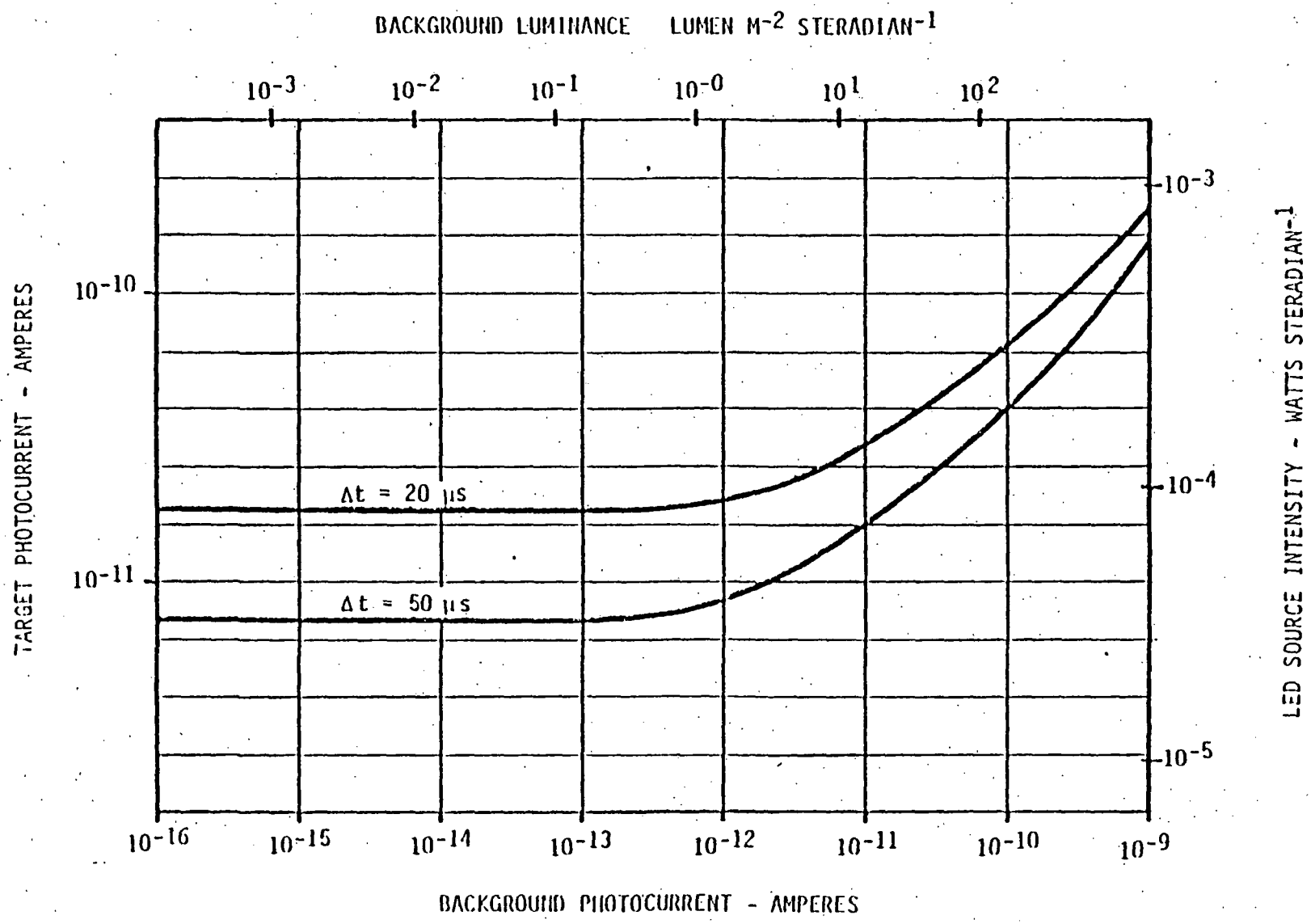

Figure 19 Target Intensity Versus Background Luminance LED Point Target λ = 655 nm
Photo Cathode Sensitivity 30 mA/watt, 200 μA/lumen
Lens f/2.8, T = 0.8
Aperture 200 x 200 μm
Sample Time 20, 50 μs
Signal-to-Noise Ratio 30:1 RMS, Noise Factor k = 2.5

There are several means available to achieve this end. First, the targets can be made the most intense source within the tunnel. LED's can be pulsed to intensity levels 20-100 times greater than their dc, 25°C ratings for 1 percent duty cycle at 300 Hz pulse rate. In this system, the target diode would be turned on only when the particular target position is being measured. This will require a small amount of circuitry in the model in addition to LED controller.

Further reduction in system susceptibility to background illumination can be obained by using narrowband optical filters on the cameras. If a filter with a passband of 50 nm centered on the 655 nm LED emission wavelength is used, the insertion loss will be about -3 dB. The out-of-band transmission is usually less than -60 dB.

With this kind of optical filter, background light due to tungsten sources would be reduced by 13 dB, cool white fluorescent sources by 19 dB, but only 0 to 3 dB for HeNe laser sources.

Added discrimination against HeNe laser light can be obtained by using a narrower bandpass and accepting a greater insertion loss or using the less efficient green LED's. The problem is the emission wavelengths of red LED's, and particularly, the high efficiency red LED's overlap the HeNe laser wavelength as shown in Figure 20.

If the narrow band optical filter does not provide sufficient discrimination between target and background, a phase coherent, modulated light system could be considered. Each of the

target LED's would be modulated at a frequency in the range of

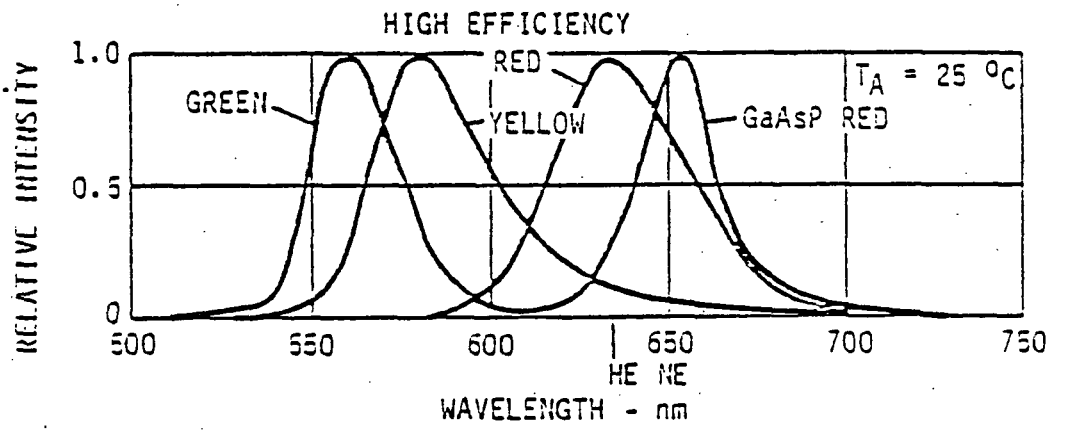

Figure 20. LED Relative Intensity Versus Wavelength

5 MHz. Since the image dissector tube will pass this frequency, a tuned amplifier, phase sensitive detector would replace the conventional preamplifier. The system would accept optical radiation within the optical filter passband having an amplitude modulation of 5 MHz and the proper phase relationship to a reference signal. This is a complicated approach and is an extreme but effective measure. This approach avoids the 20 to 60 μs time penalty associated with measuring the background. The 50 percent duty cycle of the 5 MHz modulation doubles the needed target intensity.

Angular Distribution of the Target Light

An almost hemispherical distribution of light from the target is essential.

For a flat plate at zero angle of attack, the cameras view targets at a 35° angle from normal incidence. As the flat plate changes angle of attack, the 35° angle sweeps over a range of angles from 16° to 54°. The camera has a rather wide field of

view, 34°, therefore a nominal 35° viewing angle at the center of the field of view becomes 18° to 52° at the sides of the field of view for zero angle of attack and -1° to 71° for 19° angle of attack. The greatest viewing angle is about 72° for 19° angle of attack and occurs in the corner of the field of view. If targets are mounted on curved surfaces, this can lead to still larger viewing angles.

For a target having a Lambertian distribution, the intensity varies as $\cos \theta$, where θ is the viewing angle from the normal. At $\theta = 70°$, the target intensity is only one-third of the normal value. Standard encapsulated LED's are not Lambertian. Intensity at 70° is about 10 to 20 percent of on-axis intensity. Stated differently, the brightness required for off axis viewing will determine the target source intensity. This fact alone will likely dictate pulsed operation of the LED targets.

Tracker Packaging

The packaging concept for an individual tracker is shown in Figure 4. All the optical and electrical portions will be maintained at room temperature and atmospheric pressure. The concept pictured should allow an insulated pressure vessel of adequate size to be installed in the beams surrounding the test section.

The optical system must be a custom design to fit the very restricted space inside the beam. The concept of folding the optical path should provide the 40 degree field of view needed yet fit within the space available.

The housing will be made from stainless steel with 50 mm of insulation. This should provide adequate isolation from the tunnel pressure and temperature. The tunnel's dry air supply

along with electric heaters will be controlled to assure that internal temperatures are stable.

Vibration of the tracker will be minimized by energy absorbing mounts. Analysis of the windows indicates that tilts must be less than half degree which appears to be easily achieved. Motion of the tracker affects the system in different amounts depending on the motion. Vibration in the plane of the window will simply translate the tracker and will be a very small effect. Vibration perpendicular to the window will change the tracker to object distance, but again it will be a very small effect. Vibration perpendicular to the window will change the tracker to object distance but again it will be a very small effect. Rotational type vibrations could cause noticeable effects especially if the point of nutation is near the lens system. Without a structural design to model and a good vibration spectrum, it is not possible to rule out tracker vibration problems. A structural design and analysis is beyond the scope of this report. During the actual design of the SETS, a detailed mechanical model and a vibrational analysis must be performed to ensure that no vibrational problems exist.

The location of the individual trackers in the tunnel is shown in figures 1, 2, and 3. Because of the tunnel geometry, the trackers will not be identical. Trackers 3 and 4 will view the model at a steeper angle than trackers 1, 2, 5, and 6. Even though the trackers are not identical, it is anticipated that most of the components can be made interchangeable.

RAY TRACE PROGRAM

General Program Organization

A series of computer programs have been written that trace rays in a wind tunnel. The programs are organized into three groups: initialization, tracing, and analysis. The initialization and analysis programs are specifically tailored to the Stereo Electro-Optical Tracker System of the NTF wind tunnel and are limited in scope by our computer capacity. The tracing program is not limited and can trace virtually any ray in any index field with or without shock waves.

The initialization programs load information on shock waves, ray source locations, tracker locations, and index of refraction values into various data files. While most of these programs are general routines and capable of handling any geometry, the index of refraction generating program cannot. This program can handle plane and conical shock waves only. Computer programs are available that compute the density for complex-shaped shock waves. These can be converted to produce the index field with much greater accuracy and faster than writing our own programs. Thus, the initialization programs were kept simple enough to avoid the complexities of the large aerodynamic programs that already exist, yet were versatile enough to allow meaningful ray tracing.

The tracing programs take the information generated by the initialization programs and trace rays through the wind tunnel model. The result of the ray trace is put into a data file for examination by the analysis programs. The ray tracing is performed by analyzing the medium surrounding the current ray location and stepping the ray to a new location. The process is then repeated as often as required. Subroutines handle shock waves,

optical elements, and all index calculations. The ray tracing routines will trace rays through any medium with virtually any shock wave shape. The restrictions described previously for the initialization programs are not restrictions for the ray trace programs. Virtually any ray, in almost any medium, with almost any shock wave configuration, can be traced very quickly.

The analysis programs are designed to examine the output of the ray trace. Several analysis routines are possible, but only one routine is complete. That routine traces rays through the tracker optics and describes the image location. An additional routine simply displays the ray trace results without the tracker optics. Several routines were envisioned that would further analyze the output and generate a new data file for a second pass through the ray trace routine. These two pass systems would provide much more accurate answers when large ray deviations were present.

The general program organization is shown in Figure 21; Software Module Diagram and Data Flow. Three main programs, indicated by circles, provide the basic framework. Data is provided to and from subroutines as shown by the thin arrows. The initialization program and the main ray trace program build data files as their output as shown by the large arrows. The use of data files allows the user to interrupt the normal ray trace flow to either change data values or just check them.

Figure 22 shows the geometry used for all the computer programs.

Initialization Programs

The main ray trace program utilizes data stored in several different data files. These files must be loaded with the

Figure 21 Software Module Diagram and Data Flows

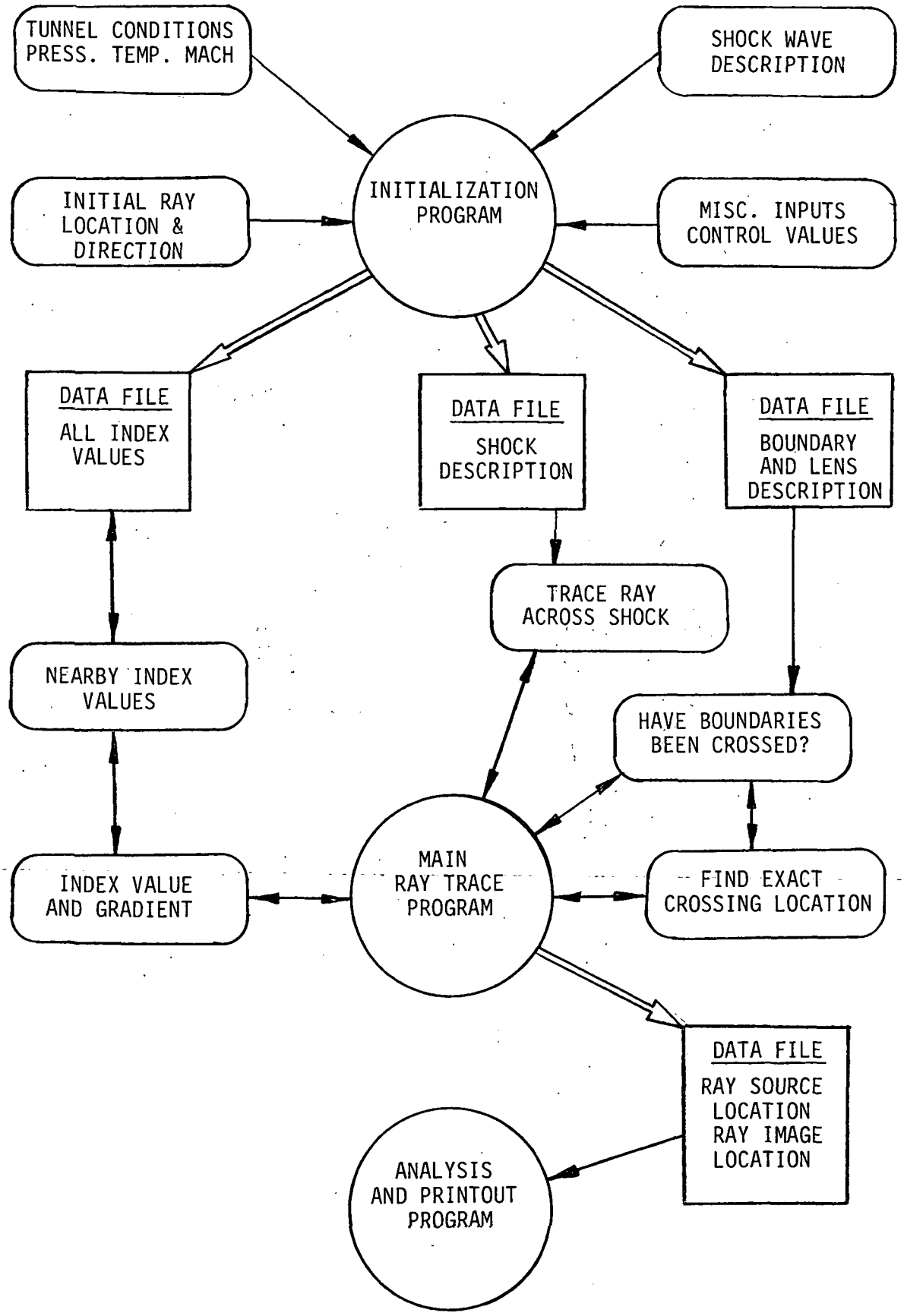

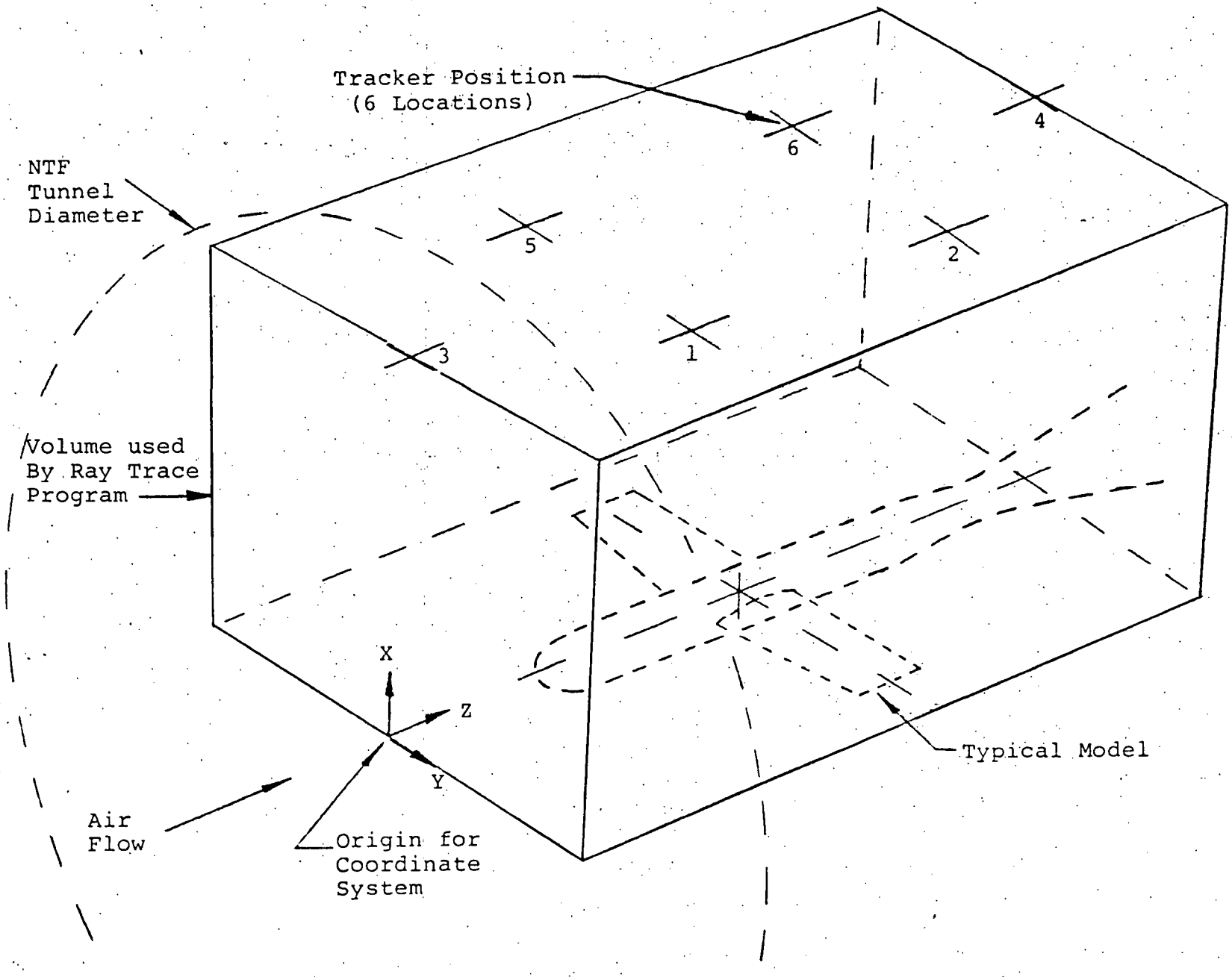

Figure 22 Ray Trace Geometry

proper data for the ray trace to be meaningful. The ray trace program does not check the input data for its scientific validity. Thus, the operator must load all the data files correctly. The computer programs described in this section are designed to assist the operator in loading and checking these input data files. There are three data files for data input. Thus, there are three groups of programs.

The first data file contains the ray source information. This file, designated as "S" file, contains the location (X, Y and Z) and initial direction (direction cosines) of each ray. There can be from one to nine rays loaded into the file. Program SBLD will load this file. The program allows the user to input individual rays or to select one of the standard ray patterns. The standard patterns are a nine-point aircraft, shown in Figure 23 and a seven-point star, shown in Figure 24. The program asks for the initial ray location and automatically calculates the direction cosines and loads it into the data file. The parameters of the particular tracker being used are also loaded into the file. Any of the six trackers shown in Figure 1 can be selected by number. All their parameters are stored in the program.

After the source file has been loaded, the contents can be examined by using program SPNT. This program prints the contents of "S" file. The values for nine rays and one tracker are listed. Any ray with a non-zero code number will be traced. The codes presently used are listed in Table 8. The tracker number is listed as its code number.

The second data file contains shock wave information. This file, designated as "W" file, contains the parameters describing all the shock waves and the optical elements. There are ten possible entries. The first seven are reserved for shock waves. Item eight and nine are automatically set to be the tunnel

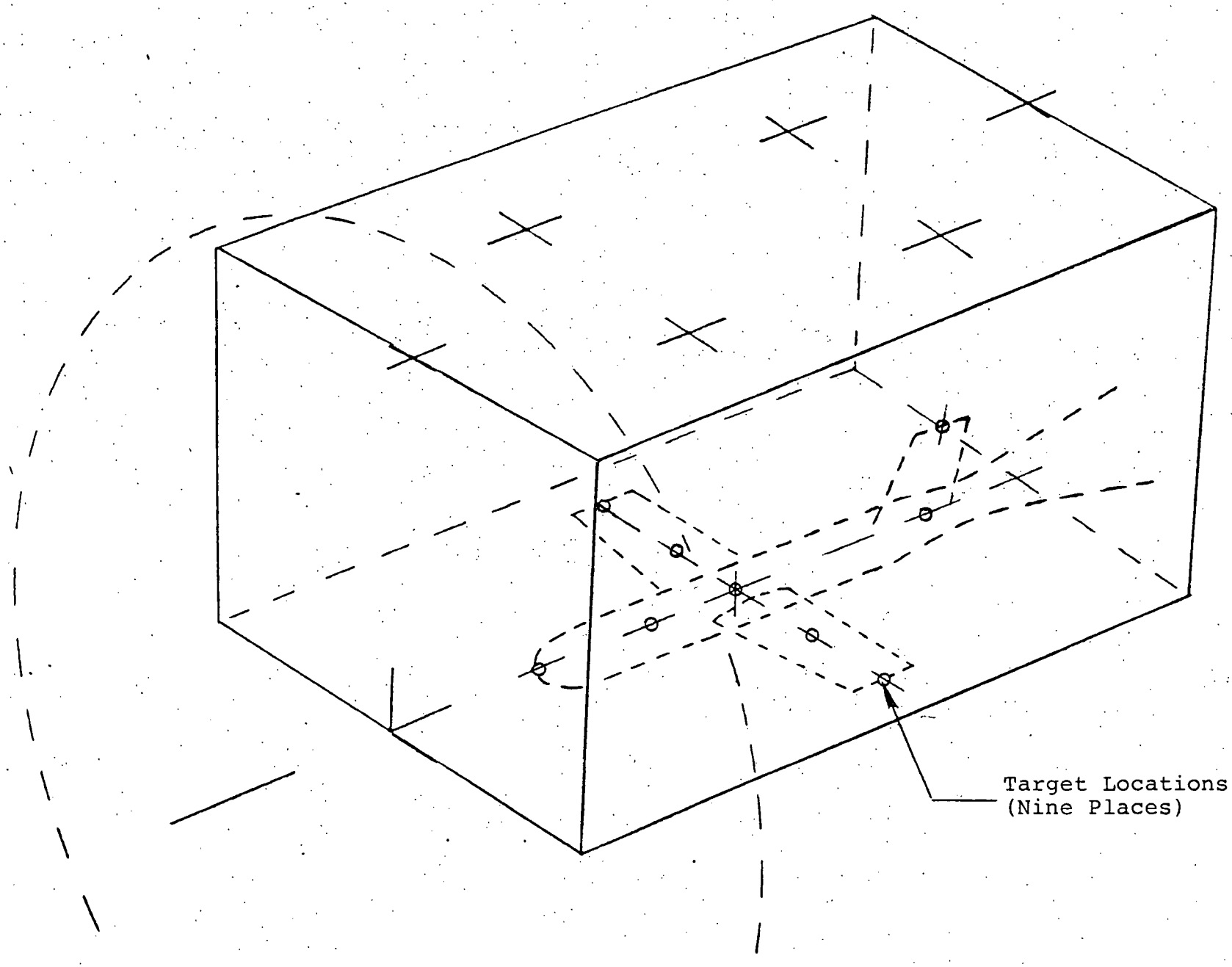

FIGURE 23: Standard Nine Point Aircraft

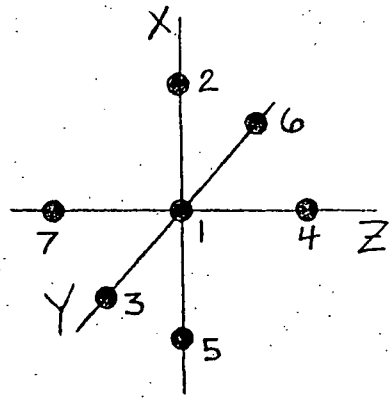

FIGURE 24 SEVEN POINT STAR PATTERN

24

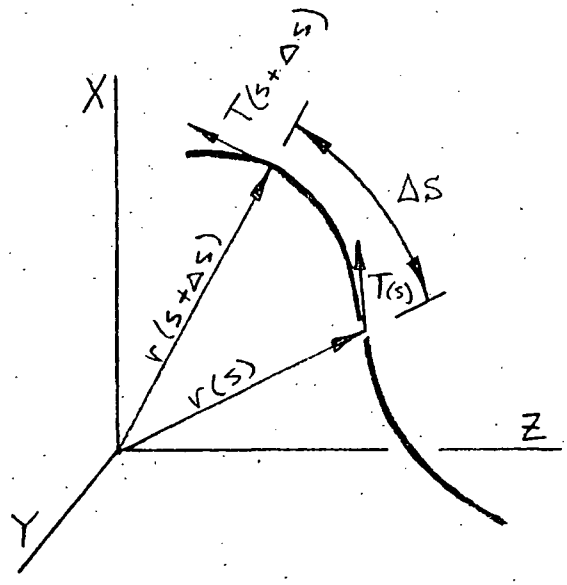

FIGURE 25 RAY VECTOR DEFINITIONS

TABLE 8 SHOCK WAVE REPRESENTATION

Cone Code = 1

$$\frac{(x-g)^2}{A^2} + \frac{(y-h)^2}{B^2} - \frac{(z-k)^2}{C^2} = 0$$

if A = B then cross section is circle

vertex at g, h, k

perpendicular is: $\frac{2(x-g)}{A^2}\hat{i}$: $\frac{2(y-h)}{B^2}\hat{j}$: $\frac{-2(z-k)}{C^2}\hat{k}$

Flat Sheet (Plane) Code = 2

$$A(x-g) + B(y-h) + C(z-k) = 0$$

point on plane = g, h, k

perpendicular is: $A\hat{i}$: $B\hat{j}$: $C\hat{k}$

Sphere Code = 3

$$(x-g)^2 + (y-h)^2 + (z-k)^2 - A^2 = 0$$

radius is A

center of g, h, k

perpendicular is: $2(x-g)\hat{i}$: $2(y-h)\hat{j}$: $2(z-k)\hat{k}$

Elliptic Paraboloid Code = 4

$$\frac{(x-g)^2}{A^2} + \frac{(y-h)^2}{B^2} - \frac{(z-k)}{C} = 0$$

if A = B then cross section is circle

vertex at g, h, k

perpendicular is: $\frac{2(x-g)}{A^2}\hat{i}$: $\frac{2(y-h)}{B^2}\hat{j}$: $\frac{-2(z-k)}{C}\hat{k}$

Hyperboloid Code = 5

$$\frac{(z-k)^2}{C^2} - \frac{(x-g)^2}{A^2} - \frac{(y-h)^2}{B^2} - 1 = 0$$

Center at g, h, k

distance from vertext to center = c

If A = B then cross section is circle

perpendicular is: $\frac{-2(x-g)}{A^2}\hat{i}$: $\frac{-2(y-h)}{B^2}\hat{j}$: $\frac{2(z-k)}{C^2}\hat{k}$

Ellipsoid Code = 6

$$\frac{(x-g)^2}{A^2} + \frac{(y-h)^2}{B^2} + \frac{(z-h)^2}{C^2} - 1 = 0$$

center at g, h, k

Semiaxes of A, B, C,

perpendicular is: $\frac{2(x-g)}{A^2}\hat{i}$: $\frac{2(y-h)}{B^2}\hat{j}$: $\frac{2(z-h)}{C^2}\hat{k}$

window. Item ten is reserved for the tracker entrance aperture and will be automatically loaded during the actual ray tracing. All shock waves and optical elements are described by a code number, three centering parameters, and three shape parameters. The code number identifies the general shape while the other six parameters give the exact mathematical formula. Any shock with a zero code number will not be used for the ray trace.

Table 8 gives the equations and parameters for each shock type. This table also gives the formula for the normal vector to the shock. This vector must be calculable whenever a ray intersects a shock wave. Using the geometry of Figure 22, the shock wave parameters must be hand calculated to best fit the actual shock being modeled. Once these values are known, program "WBLD" will allow the operator to load them into the data file.

Once the shock waves have been loaded into the data file, program WPNT will print out the contents of the data file. This allows the user to check the entries and provides a record without changing the contents of the file.

Program WTST tests the validity of the shock wave equations by plotting a cross section picture of the wind tunnel. Five cross sections are printed showing what portion of the medium has been affected by each shock. This program provides a check on each shock wave's shape and location.

The third data file contains index of refraction information. This file, designated as "N" file, contains the index of refraction at various points and the tunnel conditions. Each index value is identified by its X, Y and Z location. The "N" file contains data in blocks of 50 data points. The file can be enlarged without limit provided disk space is available. Only one block is in memory at a time so the file length is not restricted.

The "N" file is loaded by program START. This program utilizes the shock wave data file and uses supplied tunnel conditions to generate the index field. The program calculates the index on a rectangular grid throughout the area shown in Figure 22. The START program is designed to generate the index data file for simple shock waves only. It will handle plane and conical shocks only. The additional shocks listed in Table 9 procude a complex index of refraction pattern in the tunnel that the START program cannot calculate. If the additional shock shapes are required, the index (or density) distribution must be calculated (perhaps by the NASA REFRC program) and put in the "N" file. Subsequent programs for ray tracing can handle all the types of shocks listed in Table 8.

Tracing Programs

The ray tracing programs are written to handle virtually any problem yet be simple enough to allow quick answers for basic situations. The ray trace programs utilize three dimensional vector calculus thus allowing for a varying index of refraction and shock waves at compound angles. The ray is located by an X, Y, Z position and its direction of travel is direction cosines (α, β, γ). Once established, the ray is traced by a series of steps through the tunnel. The final ray location and direction is stored for analysis. Multiple rays are traced (nine in the present version) and are analyzed by themselves or in conjunction with other ray trace results.

The ray tracing is done by a single main program, called RAY, that calls on eight subroutines for various situations. The main program loads into memory the shock wave data file and the ray source data file. It loads into memory by using subroutines, the nearest index data points, computes the index gradient and steps the ray to its next location. The user

is kept informed of the ray's progress throughout its journey by periodic status checks. Additional information is printed out when shocks are crossed or an unusual situation occurs.

Ray Calculation

Figure 25 shows the vector geometry used for the ray trace. The tangent at point s is the vector T(s), and the ray location is defined by the vector r(s). The initial ray location and direction are provided by initialization programs. The index of refraction (n) is a function of location and is provided by subroutines. Thus, the differential equation for light rays can be solved:

$$\frac{d}{ds}\left(n\frac{d\vec{r}}{ds}\right) = \text{grad } n$$

Thus, $d\vec{r}/ds$ is a unit vector tangent to the light path. If this is evaluated at a point when the ray can be traced a short distance and the process repeated, the value of $\vec{r}$ gives the position of the ray (photon) at the point of interest. The value of $d\vec{r}/ds$ gives its direction of travel as the point. Thus, defining a new variable $\vec{T}$ to represent the unit tangent to the ray path makes the equation easier to understand without violating any mathematical laws.

letting: $$\vec{T} = \frac{d\vec{r}}{ds}$$

reduces the ray equation to:

$$\vec{T}\frac{dn}{ds} + n\frac{d\vec{T}}{ds} = \text{grad } n$$

176 61208-46

or: $$\frac{d\vec{T}}{ds} = \frac{1}{n} (\text{grad } n - \vec{T} \frac{dn}{ds})$$

The term dn/ds is the directional derivative of n in the direction of s. The direction of s is given by dr/ds. Thus, a unit vector in the s direction can be calculated.

$$\frac{dn}{ds} = \text{grad } n \cdot \vec{A}$$

where $\vec{A}$ is a unit vector in the s direction.

$$\vec{A} = \frac{d\vec{r}}{ds} = \vec{T}$$

Thus, $\frac{dn}{ds} = \text{grad } n \cdot \vec{T}$ which results in:

$$\frac{d\vec{T}}{ds} = \frac{1}{n} (\text{grad } n - \vec{T} (\text{grad } n \cdot \vec{T}))$$

Where all these terms are evaluated at point s.

Using this result, the tangent to the ray can be found by stepping along the ray:

$$\vec{T}(s + \Delta s) = \vec{T}(s) + \frac{d\vec{T}(s)}{ds} \Delta s$$

This equation can be thought of as the first terms of the Taylor series about a point:

$$\vec{T}(s + \Delta s) = \vec{T}(s) + \frac{d\vec{T}(s)}{ds} \Delta s + \frac{1}{2} \frac{d^2\vec{T}(s)}{ds^2} \Delta s^2 \ldots\ldots$$

or it can be thought of as the definition of a differential:

$$\frac{d\vec{T}}{ds} = \frac{\vec{T}(s + \Delta s) - \vec{T}(s)}{\Delta s}$$

which reduces to the same formula.

The location of the light ray can be found using its Taylor series expansion:

$$\vec{r}(s + \Delta s) = \vec{r}(s) + \frac{d\vec{r}(s)}{ds} \Delta s + \tfrac{1}{2} \frac{d^2\vec{r}(s)}{ds^2} \Delta s^2$$

or using previously defined symbols:

$$\vec{r}(s + \Delta s) = \vec{r}(s) + \vec{T}(s) \Delta s + \tfrac{1}{2} \frac{dT(s)}{ds} \Delta s^2$$

Thus, the ray location and direction can be calculated for each step.

Data Selection

Index of refraction data is stored on the disk in a single large data file. This file consists of blocks of 50 data points. Each data point consists of an X, Y, and Z coordinate and the index value. This file is read block by block into memory. Each block is checked for valid data points then discarded and the next block read in. This process provides a quick look at all the index data without using large amounts of memory.

As the index data file is read and checked, the 50 data points nearest the present ray location are retained. These are stored in common and are then arranged in order to distance by a subroutine. Thus, at any time the nearest data points are available.

Gradient Calculations

The index of refraction is a function of X, Y and Z. Thus, function will be approximated by a simple polynomial with four unknown coefficients. With four data points, the four unknowns can be solved for. The polynomial used is:

$$N = Ax + By + Cz + D$$

This results in a linear approximation in all three directions. The gradient can be calculated by:

$$\text{Grad } N = Ai + Bj + Ck$$

A subroutine calculates the polynomial coefficients when given four data points. The routine converges to an answer only when the four data points are not in the same plane. The four points closest to the ray may not provide a solution. When this happens, data points farther away are selected according to Table 9. If after typing all sixteen combinations in the table and a solution is not reached, the index is approximated as the average of the four closest points and the gradient set to zero. This steps the ray without any direction change and provides another attempt at solving the polynomial.

Boundary Representation

All boundaries, shock waves, and optical elements are represented by a mathematical formula. These equations are written in homogeneous form where $f(x, y, z) = 0$. The program provides for the basic conic sections listed in Table 8. Any shape that can be described by six coefficients could be modeled with only slight modification to the subroutines.

Each time the ray is stepped, the equations for each shock wave are evaluated. If it is zero, the ray is on the shock. If it is not zero, then its sign indicates what side of the boundary the ray is on. If the current ray step is across a shock, a subroutine is called and the exact crossing point is located. An interactive technique is used to find the crossing point. The equations are evaluated at a point half way between the old and new ray locations to see what side of the shock that point is on, and a new location is computed. The process is repeated until the crossing is found.

Table 9. Data Point Selection

Solution Attempt	Data Points Used							
	1	2	3	4	5	6	7	8
First	X	X	X	X				
2	X	X	X		X			
3	X	X		X	X			
4	X	X	X			X		
5	X	X		X		X		
6	X	X			X	X		
7	X		X	X	X			
8	X		X	X		X		
9	X		X		X	X		
10	X			X	X	X		
11	X	X	X				X	
12	X	X	X					X
13	X	X		X			X	
14	X	X			X		X	
15	X	X				X	X	
16	X	X					X	X

Refracting Surfaces

Shock waves and optical elements are modeled as single refracting surfaces with the index of refraction changing at the surface. The index is calculated by the gradient subroutine, and the incident angle is computed geometrically from the ray direction and the surface normal. Thus, the refracted ray angle can be calculated by Snell's law: $n \sin i = n' \sin i'$

This formula holds for three dimensions but is difficult to implement. Using the method given in Modern Geometrical Optics, by M. Herzberger, a vector solution is derived and summarized below.

The vector form of Snell's law is:

$$\vec{s} \times \vec{0} = \vec{s}' \times \vec{0}'$$

where

$\vec{s}$ = incoming ray, direction and magnitude
$\vec{s}'$ = outgoing ray, direction and magnitude
$\vec{0}$ = vector of unit length normal to shock
$\times$ = vector cross product

The ray vector ($\vec{s}$, $\vec{s}'$) can be thought of as unit vectors in the ray direction times the index of refraction. Thus:

$$\vec{s} \times \vec{0} = n \sin i \, \vec{N}$$

where

$\vec{N}$ is normal to the plane $\vec{s} \times \vec{0}$.

Thus, the original formula results in

$$n \sin i \, \vec{N} = n' \sin i' \, \vec{N}$$

Rewriting the original formula:

$$\vec{s} \times \vec{0} = \vec{s}' \times \vec{0}'$$
$$(\vec{s}' - \vec{s}) \times \vec{0} = 0$$
$$\vec{s}' - \vec{s} = K \vec{0}$$

where K is the appropriate scalar value.

176 61208-51

Solving for K:

$$K = \vec{0}\,\vec{s}' - \vec{0}\,\vec{s}$$

From the definition of dot product:

$$\vec{0}\,\vec{s}' = n' \cos i'$$

Substitute trigonometry identity $\cos x = \sqrt{1 - \sin^2 x}$

$$= n' \cos i' = n' \sqrt{1 - \sin^2 i'}$$

$$= \sqrt{n'^2 - n'^2 \sin^2 i'}$$

Substitute $n' \sin i' = n \sin i$

$$= \sqrt{n'^2 - n^2 \sin^2 i}$$

Substitute trigonometry identity: $\sin x = \sqrt{1 - \cos^2 x}$

$$= \sqrt{n'^2 - n^2 + n^2 \cos^2 i}$$

Substitute $\vec{0}\,\vec{s} = n \cos i$

$$= \sqrt{n'^2 - n^2 + (\vec{0}\,\vec{s})^2}$$

Thus, K can be calculated by:

$$K = \vec{0}\,\vec{s}' - \vec{0}\,\vec{s}$$

$$K = \sqrt{n'^2 - n^2 + (\vec{0}\,\vec{s})^2} - \vec{0}\,\vec{s}$$

and the outgoing ray found by:

$$\vec{s}' = \vec{s} + K\,\vec{0}$$

Analysis Programs

All analysis and printout programs read the data file generated by the ray trace program and print an analysis of the ray trace. The data file includes the ray starting and stopping locations, the shock wave parameters, and the general tunnel parameters.

Nine rays are traced during the execution of the ray trace program. This allows the analysis program to compute meaningful items without repeated runs of the program. In the initialization programs, options are built in for standard target locations as well as individual target selection. The standard targets represent an aircraft model and a star. These two patterns should allow quick analysis of most tunnel conditions.

The analysis program LOOP traces rays through the tracker optics and describes the image location. It also prints the tunnel conditions and other useful parameters. If time had permitted, this program would have been expanded to generate a new set of ray starting conditions for a second pass through the ray trace routine. Thus, the name LOOP. The second pass would provide more accurate answers when large ray deviations were present by forcing the rays to enter the center of the tracker's entrance aperture. The LOOP programs geometric optics approximations to calculate the ray path to the image plane.

In geometric optics, parallel rays incident on a lens are brought to a focus at the focal plane. Thus, any ray hitting the lens is just as good as any other provided they are parallel. If the chief ray is selected, the ray trace is trivial. The chief ray is the ray that goes through the center of the lens. In geometric optics, the chief ray is undeviated when passing through the lens. Figure 26 pictures the chief ray concept. This can be

thought of as a pinhole camera in that the rays are undeviated. However, the geometric optics approximation allows a ray hitting the lens off center to be traced. The farther off center, the more error introduced by the geometric approximation. Thus, the computer program may be required to retrace a ray to keep its off centering within some limit.

Figure 27 shows the elements needed to derive the ray trace equations. The center of the lens is located at X_0, Y_o, and Z_o. The optical axis has direction numbers of A, B, and C. The image plane is perpendicular to the optical axis and through the focal point. The focal point is D, E, and F and is given by:

$$D = X_o + AK$$
$$E = Y_o + BK$$
$$F = Z_o + CK$$

where K is a distance parameter found from the focal length. If A, B, and C hapen to be direction cosines rather than direction numbers, then K is the distance from the lens center to the image place. This distance is the focal length if the optics are focused at infinity. Since the restriction of making them cosines has not been applied, the value of K must be found.

$$\text{Focal length} = f = \sqrt{(X_0 - D)^2 + (Y_o - E)^2 + (Z_o - F)^2}$$

$$f = \sqrt{(AK)^2 + (BK)^2 + (CK)^2}$$

$$f = \sqrt{K^2 (A^2 + B^2 + C^2)}$$

$$f = K \sqrt{A^2 + B^2 + C^2}$$

$$K = \frac{F}{\sqrt{A^2 + B^2 + C^2}}$$

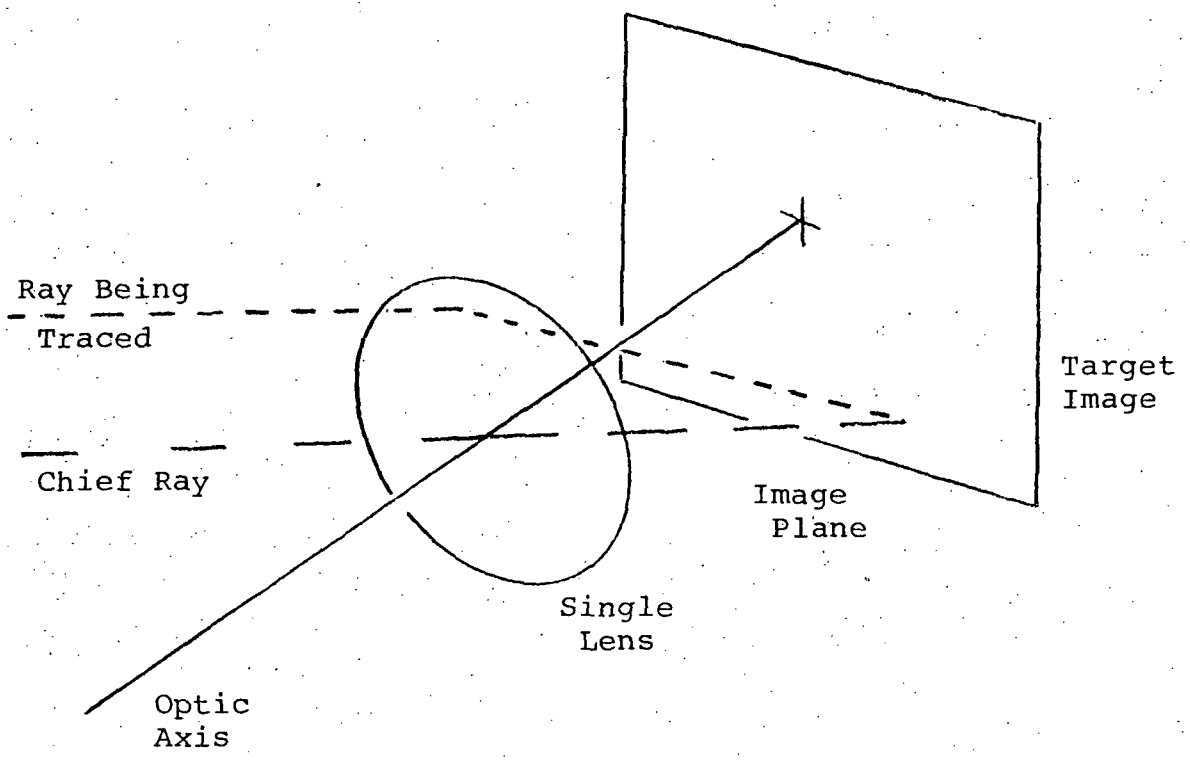

Figure 26 Geometric Optics Concept

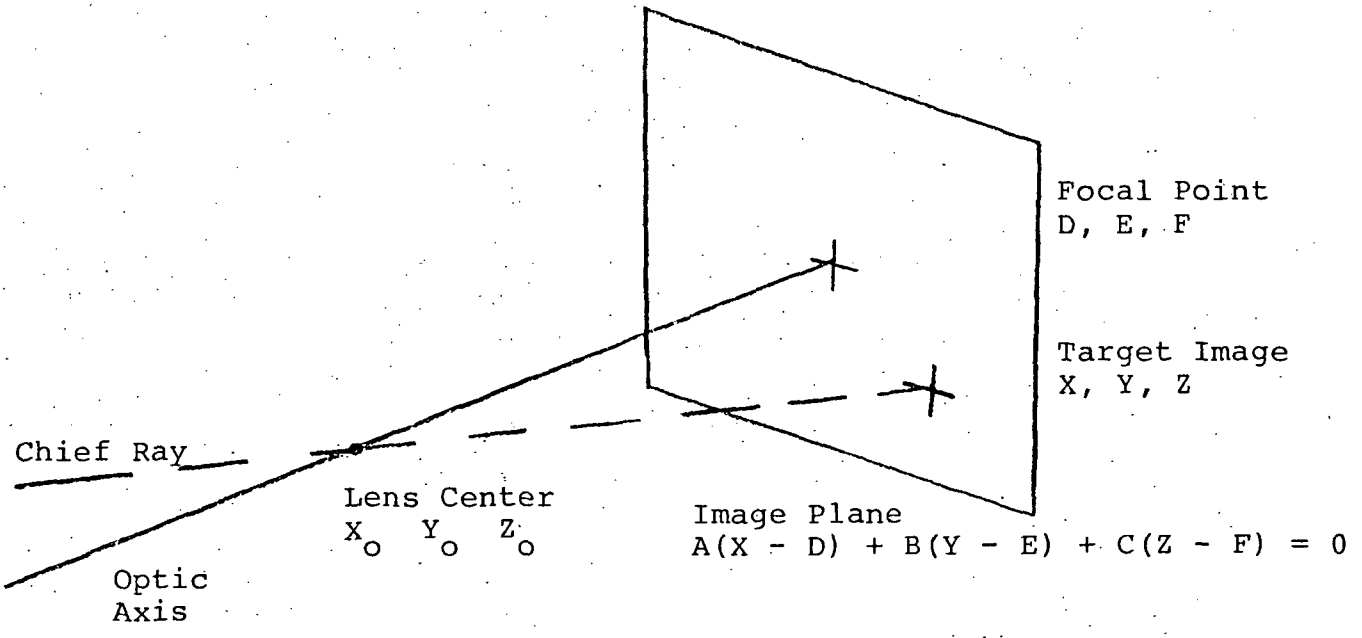

Figure 27 Ray Trace Variables

The general equation for a plane through a point with coordinates X_p, Y_p, and Z_p and perpendicular to a line with direction numbers a, b, and c is:

$$a(X - X_p) + b(Y - Y_p) + c(Z - Z_p) = 0$$

The equation of the image plane can be written as:

$$A(X - D) + B(Y - E) + C(Z - F) = 0$$

or it can be expressed as:

$$AX + BY + CZ = G$$

where G is a constant.

$$G = A(X_o + AK) + B(Y_o + BK) + C(Z_o + CK)$$

In the geometric optics approximation, the chief ray is assumed to pass through the lens center traveling in the same direction as the ray just traced through the wind tunnel. Any point on this ray can be found by:

$$X = X_o + \alpha\ell$$
$$Y = Y_o + \beta\ell$$
$$Z = Z_o + \gamma\ell$$

where X_o, Y_o, and Z_o are the lens center coordinates, α, β, γ are the ray direction numbers, and ℓ is a distance parameter. If α, β, γ happen to be direction cosines, then ℓ is the distance. The point is away from the lens center. However, the direction numbers cannot be assumed to be direction cosines.

The point where the chief ray intersects the image plane can be found by combining the two equations to yield:

$$A(X_o + \alpha\ell) + B(Y_o + \beta\ell) + C(Z_o + \gamma\ell) = G$$

this reduces to:

$$\ell = \frac{G - AX_o - BY_o - CZ_o}{A\alpha + B\beta + C\gamma}$$

The numerator is dependent on the tracker parameters only and can

be calculated ahead of time. Thus:

$$\ell = \frac{H}{A\alpha + B\beta + C\gamma}$$

The value of H can be found by substituting the value of G and solving to yield:

$$H = K(A^2 + B^2 + C^2)$$

thus:

$$\ell = \frac{K(A^2 + B^2 + C^2)}{A\alpha + B\beta + C\gamma}$$

It is interesting to note that the denominator is the dot product of the optical axis, and the chief ray and the numerator goes to unity if A, B, and C are direction cosines.

CHARGE INJECTION DEVICES

Real time measurement of aeroelastic deformation of the NTF wind tunnel models is complicated by the likely high level of mechanical vibration of the model and trackers. The concern from a measurement viewpoint is not so much with the structural design of the measurement system as it is with finding a measurement scheme whose accuracy and precision have low susceptibility to vibration.

The system concept presented in the earlier report[15] used a variation on an image dissector star tracker to measure the image plane coordinates of self luminous targets. Multiple targets are tracked in seeming real time by rapid measurement of each target image and by achieving a capability to sequentially measure a large number of targets per second. This method requires that the stereo cameras measure the same target image at the same time. Key factors affecting the performance of the system are the amplitudes and frequencies of the vibration, the number of targets which can be measured per second, and the total number of targets.

The vibration effects can be divided into two categories. Category I vibrations are those which cause the ensemble of targets to move within the system field of view. Examples of

---

[15] Hertel, Richard J.: Study of a Stereo Electro-Optical Tracker System for the Measurement of Model Aeroelastic Deformations at the National Transonic Facility. NASA CR-159146, 1979.

this vibration are the rigid body motion of the model and sting, the bending modes of the sting, the tracker mounting point vibrations causing image rotation or changes in the sensor line of sight vector. Category I vibrations can severely affect accuracy unless all target positions are measured in a time which is short compared to the vibration periods. It is category I vibrations which drive the system sequential target rate requirements and target brightness requirements.

Example of category II vibrations are the bending modes of the model. These vibrations affect the sensed spacings among the various targets. It is precisely these inter-target spacings which are the key to measuring the model deformation. It is assumed that the desired model deformation data is the average of the target positions over a period of time and not the instantaneous deformation. Using this assumption as a basis for a signal processing algorithm means obtaining a sufficient number of pseudo-random target position samples over a long enough period of time to accommodate the bending mode frequency spectrum.

An Alternate Approach

Category I vibration effects can, in principle, be substantially reduced, if not eliminated, if all target positions are measured or at least recorded at the same time. This line of reasoning generally leads to either vidicon TV systems or fast framing film cameras; neither are acceptable for this application. MOS-charge transfer devices provide an alternative sensor technology.

Developments in the field of solid state, self-scanned sensors have progressed to the level that such devices appear attractive for this application. The specific sensor device considered here is that of the charge injection device (CID) as built

by General Electric. Other devices such as charge-coupled devices (CCD) by RCA, TI or Fairchild are also worth consideration but are beyond the scope of the immediate task.

Charge Injection Devices

These are monolithic silicon sensors presently available as 128 x 128 pixels of 45 x 45 μm or 244 x 248 pixels of 36 x 46 μm. The later device is available in a camera with RS170 compatible video and sync. A 256 x 256 pixel sensor with 20 x 20 μm pixels is reported to be in development and a camera is expected in 1982. A key property of the CID is that the pixels are contiguous.

Overall System Description Using CID

The CID sensors would use the same tunnel locations and generally the same optical concepts as described in this and the previous report. By a combination of optical bandpass filters, target brightness, and lens f/number, the targets would appear as bright spots in an otherwise dark field. The optics will be adjusted deliberately off focus so that the otherwise small image of the target covers 9 pixels on the CID. This multi-pixel coverage is needed to implement the tracking algorithm. Multi-pixel coverage restricts the minimum inter-target distance for all model orientations and camera angles. If two target images merge, the signal processing algorithm becomes much more complex and may not yield a solution since targets are viewed simultaneously.

A coarse degree of real time tracking is needed in order to minimize the volume and rate of data sent to the computer. The CID tracker extracts the nine pixels associated with each target image from the full frame and only transmits these nine.

Table 10 lists the system performance objectives as they relate to a CID based system.

System Performance Analysis

The performance will be examined for three different density CID's:

- 128 x 128 pixels of 45 x 45 μm
  Available now

- 256 x 256 pixels of 20 x 20 μm
  Available early 1982

- 512 x 512 pixels of 20 x 20 μm
  Projected 1984.

CID performance data will be that of the 128 x 128 device scaled to that of the other densities. The results are summarized in Table 12.

Field of View, Lens Focal Length, and Magnification

The nominal distance from model to tracker is about 1600 mm. For simplicity, a 1 x 1 m field of view will be assumed to exist at this distance.

The required lens focal length is

$$\frac{f\ell}{1600} = \frac{\text{image size}}{\text{field of view}} = \text{Magnification}$$

176 61-18-58

Table 10. SETS Characteristics - CID Version

Sensed Volume	0.8 m by 1.4 m by 0.5 m
Target Sources, Number	5 to 50
, Type	Light-Emitting Diode
, Size	0.5 mm diameter
Model Deformation at Target Location	± 20 mm maximum
Sensor Position Deviation Detection	0.05 mm all axes
Stereo Position Deviation Calculation	0.1 mm all axes
Model Vibration Limits	± 12.5 mm at 20 Hz ± 5 mm at 50 Hz ± 1.25 mm at 200 Hz
Sensor Environment Control	70°F Dry Air at 130 psi (NASA Supplied) Electrical Heating
Tracking Electronics	Digital, in Tracker head Software, in computer
Calibration, geometric	Area map, prior to test
Pre-Test Reference	Targets on Stable Portion of model
Data Processor Type	MODCOMP
Data Storage	Magnetic Tape
Control/Display	Keyboard/Printer
Position Display	CRT Display
Hard Copy	Line Printer/Plotter

Table 11 TRACKER PERFORMANCE COMPARISON

Performance Parameter	Tracker Type IDT	128 CID	256 CID	512 CID
1. Field of View	— — — — —	—1.0 x 1.0 m — — — — — — —		
2. Targets	LED, individually pulsed	— — — —	LED, simultaneously pulsed	— — —
3. Lens Focal Length	12.5 mm	9 mm	8 mm	16 mm
4. Minimum Resolveable Target Position Change at Model (CID SNR = 64)	50 μm	125 μm	60 μm	30 μm
5. Targets/second	1500	N/A	N/A	N/A
6. Targets/Field of View	limited by model construction constraints	Limited by the number of targets that will fit within the field of view without over lap at large viewing angles.		
7. Frames/second	N/A	275	65	18
8. Maximum Data Rate to Computer	30 K bytes	200 K	40 K	23 K

Sensor (Pixel)	Image Size	Focal Length	1/M
128 x 128 (45 µm)	5.76 x 5.76 mm	9.2 mm	174
256 x 256 (20 µm)	5.12 x 5.12 mm	8.2 mm	195
512 x 512 (20 µm)	10.2 x 10.2 mm	16.4 mm	98

Target Position Determination

The objective performance is to resolve 50 µm change in position at the model. This dimension can be referred to the tracker sensor as (50 µm)(M) = d. The value of d for the respective cameras are 0.3, 0.25 and 0.50 µm.

The plan is to use a centroid finding algorithm.[12] This method uses the numerical intensity data from the 3 x 3 array of illuminated pixels to calculate the following:

11	12	13
21	22	23
31	32	33

[12] Salomon, P.M.: Charge Coupled Device (CCD) Tracker for High-Accuracy Guidance Applications. Optical Engineering, Jan/Feb., 1981, Vol. 20 No. 1, p. 135.

$$R_1 = \sum_{i=1}^{3} I_{i1} \qquad R_3 = \sum_{i=1}^{3} I_{i3}$$

$$C_1 = \sum_{j=1}^{3} I_{1j} \qquad C_3 = \sum_{i=1}^{3} I_{3j}$$

$$S = \sum_{i=1}^{3} \sum_{j=1}^{3} I_{ij}$$

The centroid offset from cell 22 is found by

$$x = k_x \frac{C_1 - C_3}{S}$$

$$y = k_y \frac{R_1 - R_3}{S}$$

when K_x and k_y are scale factors.

This algorithm, in effect, must infer the center of the target image to a small fraction of the pixel size.

Sensor	Pixel	d	Pixel/d
128	45 μm	0.3	150
256	20 μm	0.25	50
512	20 μm	0.50	40

The column pixel/d is a measure of the signal to noise ratio required to accomplish the desired measurement. Data sheets for the present 128 x 128 CID give spatial SNR = 25 typical and temporal SNR = 256 typical. These are presumably for full scale signals and are likely proportional to the signal. Observation of two 128 x 128 CID cameras would say that the 256 value is optimistic; 64 is closer to an observed, real world value.

The spatial signal-to-noise ratio is the pixel-to-pixel variation in sensitivity and dark current. These variations are presumed to be linearly correctable given two data bases; the dark current at each pixel and the normalized sensitivity at each pixel.

One would conclude that the 256 x 256 element CID might be satisfactory but the 128 x 128 element device will be severely taxed if not incapable of the desired performance. The 512 x 512 device is not expected for another two years.

Frame Rate

CID's are MOS semiconductors. Such devices have maximum clock rates of the order of 1×10^7 Hz. The 128 x 128 camera is rated at 500 K pixels per second data rate and uses a clock at 5×10^6 Hz. It is assumed that the 500 K pixel limit is a specific choice by the manufacturer to permit 30 frame/second operation and not the absolute maximum rate. A second 244 x 248 TV compatible device is available which is specified at 4.5 M pixels/seconds.

Thus, one might expect that the maximum frame rates could be 275, 65, 18 frames/ second for the 128, 256, and 512 devices.

The 65/second frame rate in conjunction with a pulsed target array will be capable of freezing the vibration motion and following the 65/2 Hz and lower frequency motion.

Data Rate to the Computer

The data rate per tracker is estimated on the folowing basis:

- 32 targets/field of view
- 9 pixels/target
- 275, 65 or 18 frames/second
- data compression to extract only the nine (9) pixels/target
- Data transmitted

    10 bits brightness/pixel
    14, 16, 18 bit brightest pixel address/target

The rate decreases because of the slower frame rates for the larger pixel count devices. If all devices are assumed to be capable of at least 30 f/second, a likely development objective for a 512 device, then the 12K rate becomes 20K.

176 61208-65

RATE CALCULATION

		128	256	512
Targets		32	32	32
pixels/target	x	9	9	9
Video bits/pixel*	x	12	11	10
		3456	3168	2880
targets		32	32	32
Address bitss/target	x	14	16	18
		448	512	576
Bits/Frame		3904	3680	3456
Frame Rate (max)	x	275	65	18
Convert to bytes	÷	8	8	8
bytes/sec		134K	30K	8K
Reserve @ 30%		40	9	2.4
Data Link Overhead @ 20%		26	6	1.6
Max Data Rate		200K	45K	12K

---

* bits/pixel = 1.44 ln (6N/F)

where F is the fraction of full scale signal the target generates. For trackers $0.25 < F \tilde{<} 0.7$

N is pixel/d

The 512 x 512 devices can likely accommodate more than 32 targets while the 128 x 128 may not be able to handle even 32 without some adjacency effects.

The image dissector tracker, operating at an average 1500 targets/second and a peak rate of 5000 targets/second, generates 9 K bytes to 30 K bytes/second.

Target Address	32 bits
Reserve and data	16 bits
Link overhead @ 50%	
	48 bits = 6 bytes

Hardware Differences Between CID and IDT Approaches

Both sensor approaches can use the same concept of packaging; a temperature controlled, pressure isolation vessel. The circuitry, which is internal to the vessel, is quite different for the two cases.

The IDT is an active tracker whose task is to maintain lock on multiple targets, measure their position, and transmit position data to the computer via a serial data link. There is analog and digital circuitry present, A/D and D/A converters, and a signal processor for the tracking function. There will be parallel-to-serial data buffers for the coordinate data.

The CID approach will have mainly digital circuitry, and probably one or two full frame memories, to buffer the CID from the signal processor. The signal processing module will sense the brightest pixel of a group of nine and format the data for transmission.

At the computer end of the data link, so long as the CID and IDT data rates are compatible, there will be little hardware impact.

Software Differences Between CID and IDT Approach

There will be significant software differences because the IDT provides target coordinates, whereas the CID concept does not. The CID data must be processed by the interpolation algorithm to extract target centroid data. This process is presently assigned to the computer and is intended to be a post processing task because of the number of unknowns associated with dark signal and pixel-to-pixel sensitivity variation corrections required.

Data Link

The hardware section cited the use of a serial data link for both IDT and CID. The concept is to use two separate lines for the data link; one is data from the computer, the other is data to the computer. Each tracker would have its own pair of lines for a total of 12 plus 2 for the LED controller. (Power lines are additional.)

The data rate estimates for the IDT and 256 CID are both of the order of 50K bytes/sec. Harris Semi-conductor makes an Ayschronous Serial Manchester Code Adapter (HD-6408) capable of encoding and decoding high speed (100K byte per second) asynchronous serial data streams. A computer/tracker data link based on this device is illustrated in Figure 28. The clock rate illustrated is the maximum for the device and corresponds to a 100K byte/second rate. Aside from the data source, the signals controlling the latch, and the start of transmission, the scheme illustrated will suffice for either the IDT or CID sensor approach.

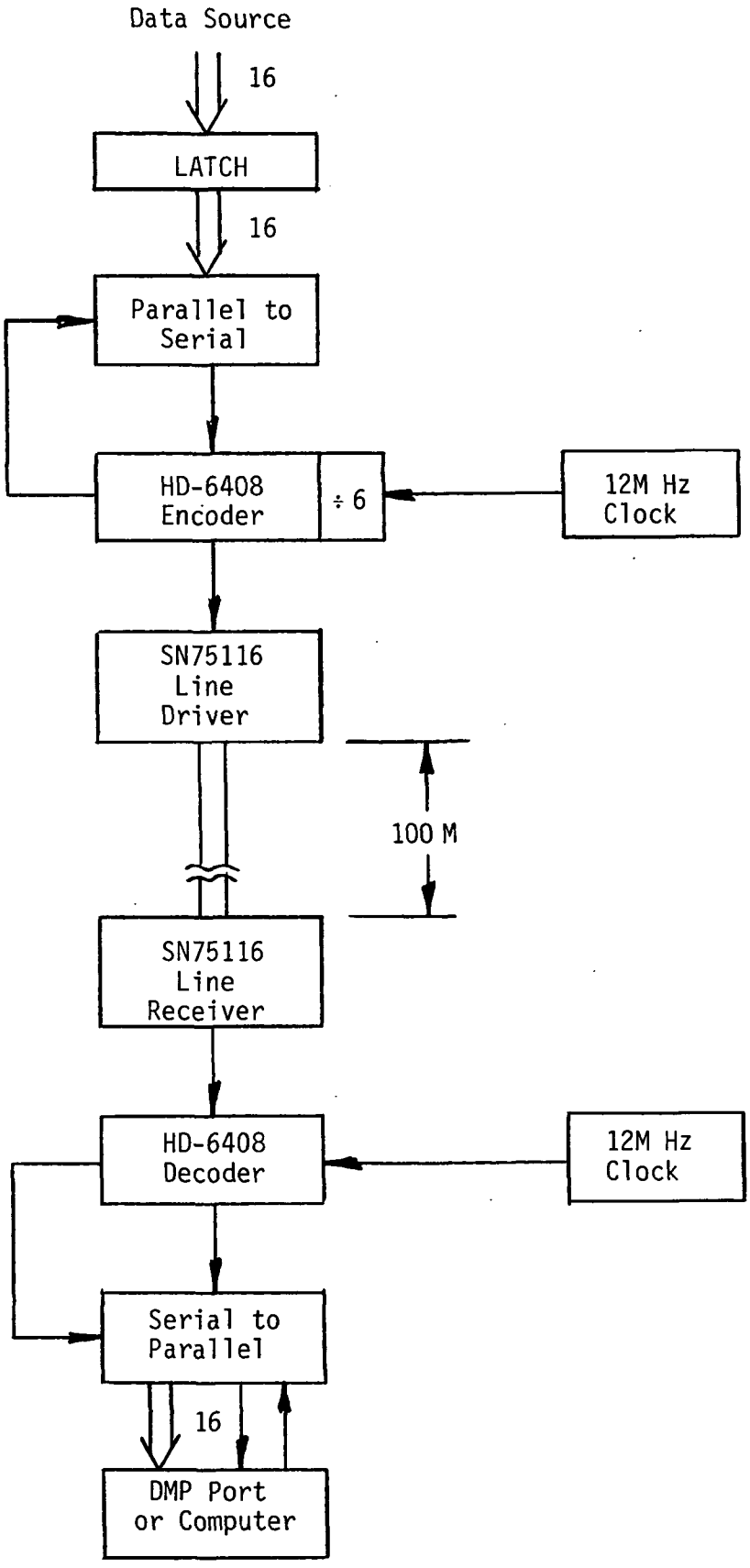

Figure 28.

100 K byte/second Data Link for Either IDT or CID Tracker

In either case, the computer is expected to receive its input via a direct memory processor. Data from the computer will likely be via a register I/O port and at a lower rate. The same link can be used for the data to the trackers or LED controller but likely at a slower clock rate.

Data given in a Texas Instruments application note shows that a link such as this composed of SN75116 drivers and receivers and using Beldon 8795 wire will accommodate 2.5 M byte rates at 100 meters.

DISTORTION CORRECTION

The SETS camera, optics and associated windows will introduce distortion into the SETS data. A correction for this distortion will be made using the raw data directly from the SETS before any stereo transformations are made. A correction prior to the stereo transformation is required because the distortions introduced are angular errors rather than positional errors. Since the SETS tracker is, in essence, an angle measuring device, the correction should be applied directly to its data.

The distortion from the optics and the camera cause the image to appear slightly displaced from its expected position on the image plane. These shifts would directly affect the accuracy of the system if they were not corrected. Some distortion is present in all optical and camera systems and does not necessarily indicate a design or construction problem. The SETS can easily incorporate a distortion correction method since the data is already digitized and stored in the computer.

Camera and Camera Lens Effects Upon System Precision

The camera and lens act in several ways to limit the system precision. The simplest limitation to understand is the one due to small but finite sized deflection increments. The demonstration system, described in the Final Report for the SETS, NASA Report Number 159146, used 13-bit deflection D/A converters over a 4.1 x 4.1 mm field of view. The minimum step size was 0.5 m at the camera faceplate. The system design concept presented in this report uses a 10 x 10 mm working field of view. Fourteen and 15-bit converters provide 0.8 to 0.4 μm increments, respectively, while covering a 12.5 x 12.5 mm scanable field of view. Such converters are available for the camera.

D/A converters and cameras have temperature dependencies which affect the size of the area scanned and the stability of the scan center within the field of view. A change in scan size is equivalent to a change in scale factor at the camera faceplate. The magnitude of the error is equal to the distance from the center of the field of view times a $\pm$ 20 ppm/°C temperature coefficient. Values range from zero at the center to $\pm$ 0.12 µm/°C at the edge of the field of view.

The centering term is $\pm$ 10 ppm/°C of the full scale size of $\pm$ 10 x 10^{-6} x 12.5 mm = $\pm$ 0.12 µm/°C. All coordinates within the field of view are equally affected by this factor. The pressure isolation container used to house the cameras must have temperature control because of the -195°C to 95°C tunnel environment. The temperature coefficients require the control of the temperature, at certain key locations in the container, be the order of plus or minus 1°C to 2°C.

The mechanical packaging of the camera and its lens must prevent shifts of the tube relative to the focal plane or coil system. The need is for less than $\pm$ 0.5 µm instabilities, a value consistent with the needs of precision star trackers used for space flight.

The camera and lens both introduce distortions of the field of view. Figure 29 shows the magnified distortion of an uncorrected image dissector camera without lens. It is assumed the lens distortion is comparable or less in magnitude. The dotted boxes are on a 1 mm grid and centered on the true position. The distance from the center to the side of the smaller boxes is $\pm$ 25 µm; $\pm$ 40 µm for the larger boxes.

This distortion is, in principle, correctable using a lookup table and interpolating between table entries. A key question is, how large must the table be in order to correct $\pm$ 0.5 μm?

Consider a group of four boxes in Figure 30 whose centers are denoted by A, B, C, and D. The distance between AB is 2 mm, and the same holds for CD. Assume the x and y position errors are known by measurement for the four positions. The position error for any point E inside the rectangle ACBD as shown in Figure 30 can then be calculated by interpolation using

$$E_x = k_1 C_x + (1 - k_1)\, D_x$$
$$E_y = k_2 A_y + (1 - k_2)\, B_y$$

where the subscript denotes the component of the error and k_1, k_2 is the position of point E from C and A, respectively.

Analysis of the 157 points in Figure 29 showed E_x and E_y calculated by interpolation different from the measured values for E_x and E_y by $\pm$ 2 μm typically and $\pm$ 4 μm at the greatest.

Assume the interpolation error is proportional to the area of the ACBD cell. Then a $\pm$ 0.5 μm interpolation error can be achieved using $(2)^2 \times 0.5/4 = 0.25$ mm^2, 0.5 x 0.5 mm cell. The 12.5 x 12.5 mm will be mapped to a sufficient density using $(12.5)^2/(0.25) = 625$ points.

System Calibration

An array of approximately 625 points will be placed in object space where the aircraft model would be. The location of each point will be measured, and the correction required will be calculated. These measurements will be the data base for all distortion correction. Since the data is taken using the entire system, it will remove the distortions from the windows, optics

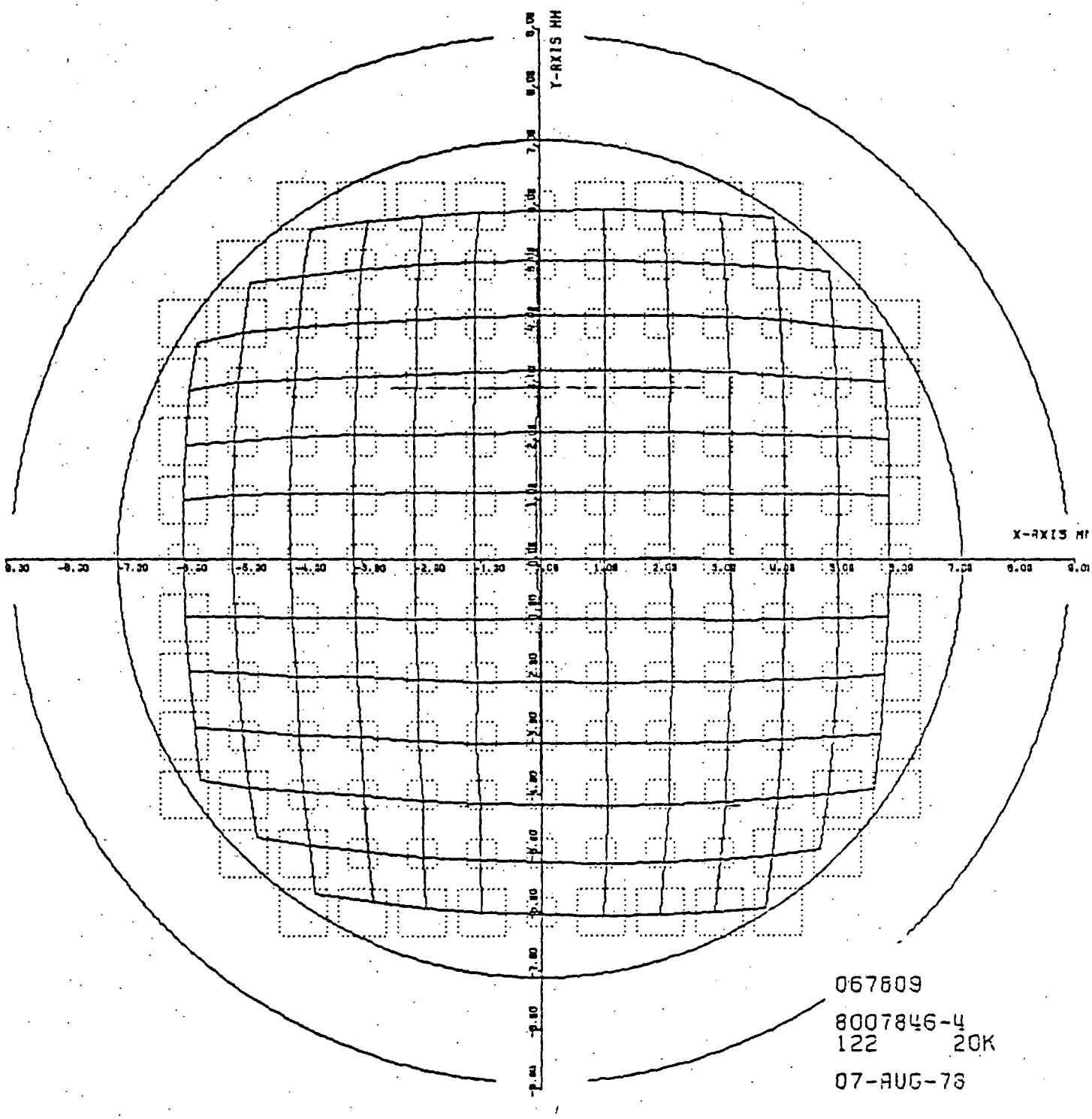

Figure 29 10X Magnified Camera Deflection Distortion for a Camera Using 25 mm Image Dissector Tube Having a 200 μm Aperture

and camera in one step. These corrections are valid for the tracker until it is physically modified or adjusted. Periodic calibration may be required due to aging and the abusive environment of the tunnel.

Due to the extreme temperature and pressure range the tracker experiences, it may be necessary to have calibrations under various conditions. If this does become necessary, a data set can be taken for various conditions and the correct set used for each data run. There would be no additional post processing time required, but the initial measurement of the calibration data sets would take more time.

Post Processing

Since the calibration data consists of measurements of specific points, some method of applying it to a random point is required. Previous sections showed that linear interpolation is adequate and the method presented there is the simplest form of interpolation and is quickly computed. Even though four data points are used (A, B, C, and D), only two (A and B) are used for the X direction and two (C and D) for the Y direction. This utilizes only half of the data available, as the y errors at A and B and the x errors at C and D are not used. It also makes the X and Y corrections independent as separate points are used for each. The interpolation is least accurate for the x correction when the point is near A or B and is least accurate for the Y correction when near C or D. This can be demonstrated by Figure 31. When point E is near point A, the X axis correction can be found using either CD or FG. Both pairs will predict the value at E yet only one pair is used. The Y value at E is known exactly as it is measured at point A. Thus, while this method may be the easiest

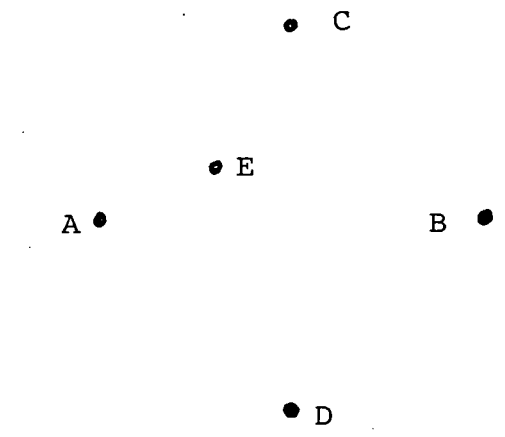

FIGURE 30 Estimate Point E Using Points A, B, C and D

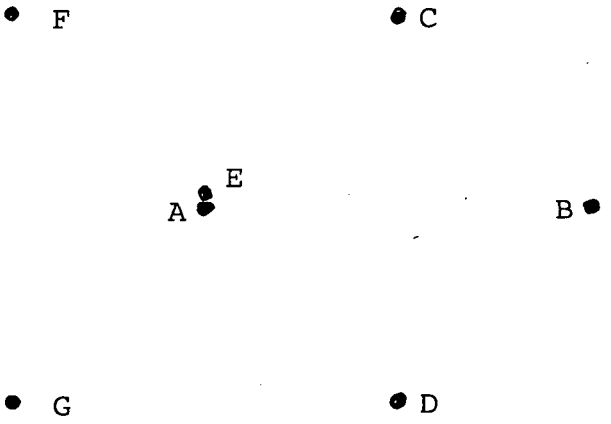

FIGURE 31 Point E Close to Point A

to compute, it does not efficiently utilize the data available and introduces some unwanted effects.

A preferred method utilizes all four data points for both the x and y corrections. This can be done by fitting a polynomial to the four data points. Thus, the error in the x direction at a point (x, y) is: Error = $C_1X + C_2Y + C_3XY + C_4$, where the coefficients are evaluated for the direction. A similar equation provides the error in the Y direction. Using four data points, the four coefficients for each direction can be found. The matrix form of the four equations is:

$$\begin{bmatrix} E_{X1} \\ E_{X2} \\ E_{X3} \\ E_{X4} \end{bmatrix} = \begin{bmatrix} C_1 \\ C_2 \\ C_3 \\ C_4 \end{bmatrix} \begin{bmatrix} X_1 & Y_1 & X_1Y_1 & 1 \\ X_2 & Y_2 & X_2Y_2 & 1 \\ X_3 & Y_3 & X_3Y_3 & 1 \\ X_4 & Y_4 & X_4Y_4 & 1 \end{bmatrix}$$

Using matrix manipulations, the coefficients can be found and the polynomial used to find the error.

The polynomial contains a linear term in X, a linear term in Y, and a cross term of XY. This combination generates a true linear approximation. The cross term does not introduce a higher order correction as might be expected.

For true linear interpolation, the value is that predicted by drawing a straight line between the data points. Figure 32 shows the process involved. The four corner points (A, B, C, and D) are measured data points. From these four points, the error is found at four points on the edge of the square with the same X or Y coordinate as the final point. The error at the final point is then estimated both vertically and horizontally. These

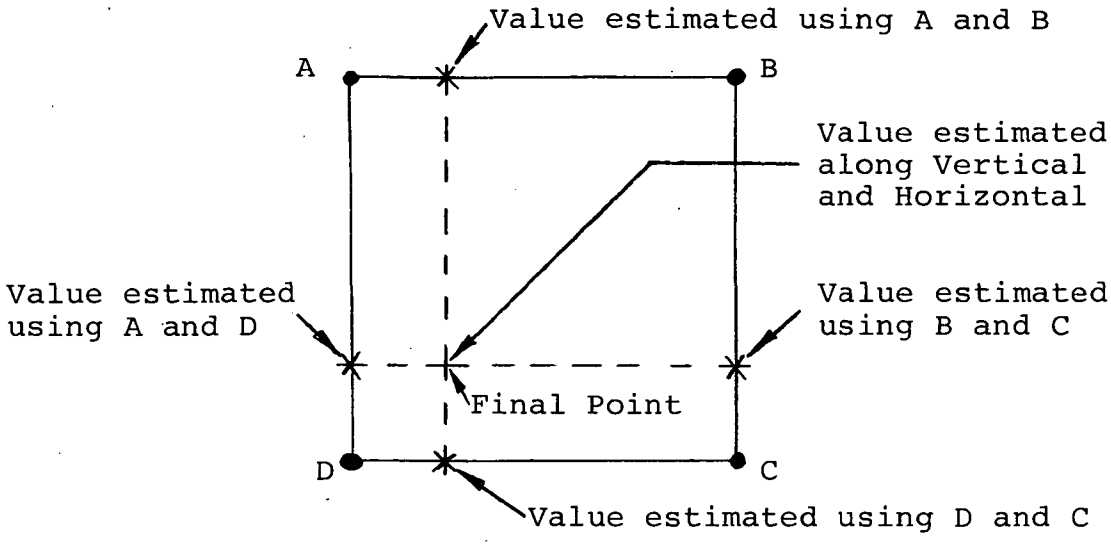

FIGURE 32 Linear Interpolation

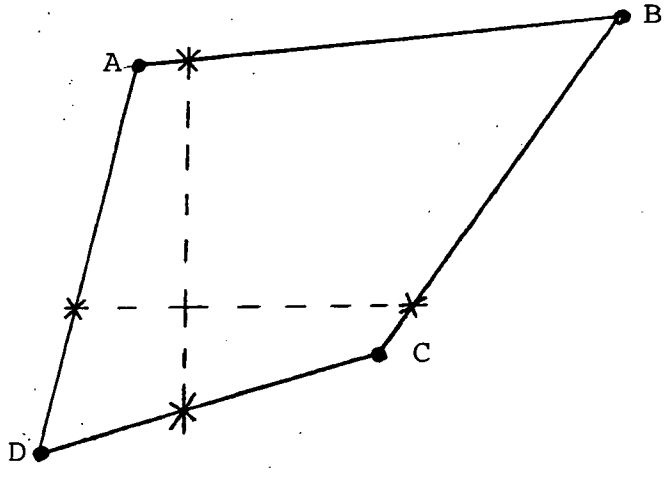

FIGURE 33 Random Data Point Interpolation

two estimates are always the same even though they are arrived at by different means. This method can be expanded as shown in Figure 33 for any four random points. All of the interpolation is the same, only the mathematics is more complex.

The polynomial approximation provides exactly the same answer as the linear interpolation method. Figure 34 is a graphical representation of the linear interpolation method. The X-Y plane is the location of the point, and the vertical is the magnitude of the error. The error is known at the four corners (A, B, C, and D) and is found everywhere else by using straight lines that are parallel to either the X or Y axis. The polynomial is the equation of the surface of all such approximations. This can be seen by holding either X or Y at a constant value:

$$\text{Error} = C_1X + C_5 + C_6X + C_4$$

which reduces to

$$\text{Error} = (C_1 + C_6)X + C_4 + C_5$$

which is a straight line of the form $E = mx + b$. Thus, the two methods produce identical results, but the polynomial method has distinct computational advantages.

Using the polynomial approach allows the data points to be randomly located without increasing the computation time. This allows an automated system to select points or dicard bad data points. If there is an area of particular concern, either for better data or a difficult distortion area, additional data points can be collected in that area. A computer program was written in FORTRAN IV using matrix manipulations to solve the four point polynomial. Each solution requires approximately 160 milliseconds or about six per second. With the SETS taking data at a rate of 1800 targets per second, a one-second data run would require about 10 minutes of post processing. This time can be reduced drastically if the polynomial for each area is computed once and then stored for use should a point again fall in that area.

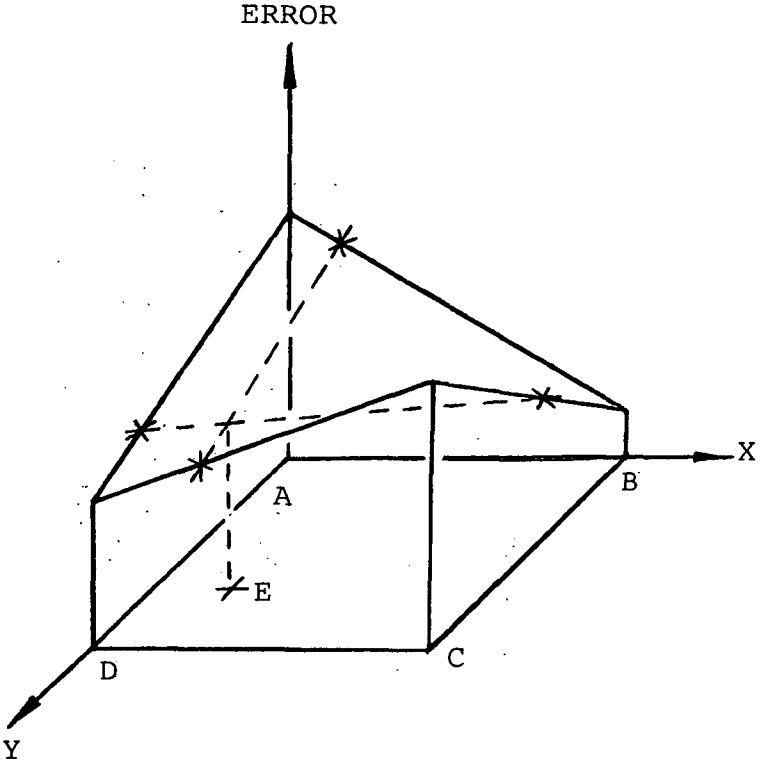

FIGURE 34 Four Point Linear Interpolation

CONCLUSIONS AND RECOMMENDATIONS

None of the error sources examined would prevent meaningful measurements of model deformations through the use of the Stereo Electro-Optical System, provided care is taken in its design and adequate post-processing of the data is performed. Detailed analysis of the actual design should minimize most of the errors to acceptable levels. Vibration of the tracker may prove to be the most difficult area to minimize due to the complex nature of the problem and the uncertainty of the vibrational environment. Shock waves can produce large errors that are correctable, provided the exact location of the shock is known. This post processing to remove shock-introduced errors is essential and depends on knowing the shock wave locations and shapes. Without this correction, or one based on assumed locations, the system performance will be limited.

Table 12 lists the possible errors when viewing a model using the Stereo Electro-Optical System. All the areas of concern can either be corrected or are small and do not degrade system performance. All of the corrections require accurate information about the tunnel conditions at the time the data was taken. Much of this information is readily available such as tunnel pressure, temperature, Mach number and Reynolds number. Some of the information may be available only after the tunnel data run has been analyzed.

The windows on the tunnel wall and in the tracker are distorted due to pressure and temperature. The flat windows become very weak lenses. The effect is to slightly defocus the image. The defocus is such a slight amount that it is insignificant. Tunnel window tilts relative to the optical axis produce a shift in the target location that could equal the entire error budget of 150 micrometers if the tilt were severe (half degree).

TABLE 12. SUMMARY OF POSSIBLE TUNNEL INACCURACIES

Error Source	Method of Error Generation	Error Produced (Acceptable Total Error Budget = 150 μm)
Windows	Pressure and Temperature produce lens and may tilt window	Insignificant lens effects (1.8×10^{11} mm F1) Half degree tilt equals entire error budget (150 μm)
Bulk Medium	Pressure and Temperature change index	Model appears to change scale (Worst Case is 4% larger) and in a nonlinear fashion. These errors can be predicted and corrected.
Laminar Boundary Layer	Gradual change in index near surface	Layer on tunnel window produces significant defocus. Layer on model produces slight (4.5 μm) shift into surface and insignificant (1 μm) along surface.
Turbulent Boundary Layer	Fluctuating index changes near surface	Layer on tunnel window reduces optical resolution to 1 mm (twice target size) but has very minor affect on system resolution. Layer on model produces a small random target shift of 10 μm.
Shock Waves	Step change in index	Error dependent on shock strength and location of data can be corrected if shock parameters are known. Curved shocks produce significant focus shifts (100 μm in focus). Correction required is proportional to distance from target to shock - Attached Shock (normal, 10mm range): 3 μm Typical Shock (45° shock, 700mm range): 100 μm Worst Case (normal shock, 1000mm range): 3 mm
Vibration	Motion between and during tracker sampling	Uniform sampling of sine wave vibration produces errors. All trackers must be synchronoized to sample simultaneously. Vibration increases measurement time. Low frequency vibration requires longer sampling times. Random sampling reduces errors.
Target Intensity	Low target to background contrast	Low intensity increases measurement time.

Care in the design should prohibit severe tilting to limit the error introduced to well below allowable limits.

Changes in the pressure and temperature of the tunnel atmosphere have a direct impact on the target location as seen by the tracker. Both increasing the pressure and decreasing the temperature cause the atmosphere to become more dense and thus increases the optical index. This increase causes the rays to bend at the windows in a non-linear fashion. The model appears to grow (4 percent in the worst case) but not uniformly. Some portions will grow as much as 9 percent while other sections grow only 1 percent. The data can be corrected to remove this effect, provided the tunnel conditions are known.

Laminar boundary layers on surfaces produce a gradual change in the optical index. This gradient causes the light path to bend depending on the properties of the layer and the incident shift in the focus. A layer on the model will cause a target to appear displaced horizontally and into the model. The apparent displacements are much smaller than the system resolution and will not be a problem.

Turbulent boundary layers on surfaces produce a fluctuating optical index causing the ray path to change randomly. If the layer is on the tunnel window, the fluctuations cause the image to blur reducing the optical resolution. The degraded resolution is still well within the design limits. If the layer is on the model, it produces a small random shift that will not affect system performance.

Shock waves produce a sharp change in the optical index and act as single refracting surfaces which bend the optical

rays. The amount of bending and the effect on the optical ray depends on the shock strength, the angle of incidence between the shock and the ray, and the distance from the model at which the ray intersects the shock. Optical rays intersecting shocks near the model are only slightly affected and correction is not necessary. Rays which intersect shocks near the tunnel window will be significantly affected and must be corrected. Correction can be made however, only if the strength, shape and location of the shock on the model are known. Curved shocks produce a lens effect which cause the point at which the target image is focused to change. This focus shift may or may not be significant depending on the individual shock.

Motion of the tracker or the target during a sampling period introduces a slight error into the convergence routine. Since the target is sampled several times to get its location, any motion during the sequence leads to errors and may require additional samples. Based on the vibration levels predicted by NASA, acceptable accuracy and sample times are expected.

Motion of the tracker or the target between sample periods can lead to large errors if all trackers do not sample simultaneously. Additional problems could develop if both the sampling and the vibration are periodic. They could combine to produce stroboscopic effects that could give errors. Low frequency vibration can also produce errors if the data collection times are short compared to the period of the vibration. The sampling technique proposed reduces all these errors to acceptable levels by adjusting the data collection time, varying the target order, and synchronizing all the trackers.

Low target intensities can lead to problems as the convergence time increases. The target and background levels

anticipated should provide adequate signal-to-noise ratios for normal operation.

The influences on tracking accuracy of the factors cited above appear to be definable to the extent of describing the general level of the effect on system output.

The use of a 128 x 128 pixel CID-type system does not appear practical. If the technology advances as expected, it will be a realistic alternative in the future. It is possible to design a data link that is device independent to allow for future system improvements.

The computer program developed does trace virtually any ray through the complex tunnel conditions. The program can handle shock wave, boundary layers, pressures, temperatures, nonhomogeneous index of refraction, and optics of any conic section or polynomial of sixth order or less. The program does approach the goal of a universal ray trace program capable of handling any tunnel condition or ray geometry.

With the cautions noted to limit window tilt and other causes, it now appears that the typical range of effects anticipated for the NTF do not preclude successful operation of the tracking system.